



NIH Public Access

Author Manuscript

Biochemistry. Author manuscript; available in PMC 2012 August 30.

Published in final edited form as:

Biochemistry. 2011 August 30; 50(34): 7361–7374. doi:10.1021/bi200923k.

Modulating Distal Cavities in the α and β Subunits of Human HbA Reveals the Primary Ligand Migration Pathway[†]

Ivan Birukou[#], David H. Maillett[‡], Anastasiya Birukova[§], and John S. Olson^{*}

Department of Biochemistry and Cell Biology and the W. M. Keck Center for Computational Biology, Rice University, Houston, Texas 77005

Abstract

The free volume in the active site of human HbA plays a crucial role in governing the bimolecular rates of O₂, CO, and NO binding, the fraction of geminate ligand recombination, and the rate of NO dioxygenation by the oxygenated complex. We have decreased the size of the distal pocket by mutating Leu(B10), Val(E11) and Leu(G8) to Phe and Trp and of other more internal cavities by filling them with Xe at high gas pressures. Increasing the size of the B10 side chain reduces bimolecular rates of ligand binding nearly 5,000-fold and inhibits CO geminate recombination due to both reduction of the capture volume in the distal pocket and direct steric hindrance of Fe-ligand bond formation. Phe and Trp(E11) mutations also cause a decrease in distal pocket volume but, at the same time, increase access to the Fe atom due to the loss of the γ 2 CH₃ group of the native Val(E11) side chain. The net result of these E11 substitutions is a dramatic increase in geminate recombination because dissociated CO is sequestered close to the Fe atom and can rapidly rebind without steric resistance. However, the bimolecular rate constants for ligand binding to the Phe and Trp(E11) mutants are decreased 5–30-fold, due to a smaller capture volume. Geminate and bimolecular kinetic parameters for Phe and Trp(G8) mutants are similar to those for the native HbA subunits because the aromatic rings at this position cause little change in distal pocket volume and because ligands do not move past this position into the globin interior of wild-type HbA subunits. The latter conclusion is verified by the observation that Xe binding to the α and β Hb subunits has little effect on either geminate or bimolecular ligand rebinding. All of these experimental results argue strongly against alternative ligand migration pathways that involve movements through the protein interior in HbA. Instead, ligands appear to enter through the His(E7) gate and are captured directly in the distal cavity.

Keywords

hemoglobin; myoglobin; xenon binding sites; geminate recombination; flash photolysis; ligand migration pathways; non-covalent binding site

The existence of internal cavities in proteins was first discovered in sperm whale myoglobin. In 1965, Kendrew's group (1) and then, in 1985, Petsko and coworkers (2) reported crystal structures of Mb containing bound Xe. These Xe sites are found in the proximal part of the heme pocket just below pyrrole ring B (called Xe1), behind the heme next to the vinyl group

[†]This work was supported by NIH Grants GM035649, HL047020, and Grant C0612 from the Robert A. Welch Foundation (to J. S. O.) and a Welch Foundation Predoctoral Fellowship (to I.B.).

^{*}CORRESPONDING AUTHOR FOOTNOTE. John S. Olson, PhD, 6100 Main Street, Houston, Texas 77005-1892; Tel: 713-348-4762; Fax: 713-348-5154; olson@rice.edu.

[#]Current address: Department of Biochemistry, 307 Research Drive, Duke University Medical College, Durham, NC 27710.

[‡]Current address: Senior Biologist, Edwards Lifesciences, LLC, One Edwards Way, Irvine, CA 92614.

[§]Current address: Department of Cell Biology, 307 Research Drive, Duke University Medical College, Durham, NC 27710.

of pyrrole B (Xe2), in the back of the distal pocket (Xe4), and between the EF corner and the H helix (Xe3). Later, it was demonstrated that these Xe cavities are involved in the kinetics of internal ligand movement after photolysis of Mb-ligand complexes (3–8). Molecular modeling and dynamics simulations went further and predicted that these apolar cavities may function as transient stations for ligands migrating from the solvent to the active site in Mb (9–14). However, most experimental data, including exhaustive mutagenesis mapping and time resolved X-ray crystallography, do not support these theoretical conclusions and suggest, instead, that ligands enter and escape Mb by the His(E7) gate pathway (3, 4, 15–21). Xe cavities are also present in the interior of HbI from the blood clam *Scapharca inequivalvis* (HbI), can trap photodissociated CO, and have been proposed to be part of the ligand migration pathway in this mollusc globin. However, blocking these docking sites with Xe, organic halides, and space-filling Phe and Trp mutations causes no appreciable change in the fraction of ligand escape from the protein. Instead, ligands appear to enter and escape the clam Hb through the distal histidine gate (22, 23).

However, the His(E7) channel is not the universal pathway for ligand movement into all globins. In some bacterial truncated hemoglobins and the neuronal mini-globin from the *Nemertean* sea worm *Cerebratulus lacteus*, ligands enter the protein through an apolar tunnel between the C-terminal ends of the E and H helices (24). In *Cerebratulus lacteus* Hb (CerHb) either blocking the apolar tunnel with Trp mutations or filling the tunnel with Xe markedly decreases both the fraction of ligand escape to solvent and the bimolecular rate constant for ligand entry into the active site (25, 26).

There is much less experimental information regarding the functional role of internal cavities in human HbA subunits. Adachi *et al.* (27) demonstrated, that after CO photodissociation, an electron density feature corresponding to the ligand was observed in the primary docking site, located 3.5 Å away from the Fe atom and above the pyrrole C ring in α subunits of human HbA. In β subunits, a similar primary photodissociated site is occupied, and a second small ligand electron density peak is found in the back of the distal pocket, ~ 8.5 Å from Fe, in a cavity circumscribed by the B10, E11, E12 and G8 amino acid side chains.

Sottini *et al.* (28, 29) measured CO rebinding kinetics in R-state HbCO that was encapsulated in silicon hydrogels in the presence of 80% glycerol and observed two geminate phases with characteristic rebinding times of $\sim 10^{-8}$ and 10^{-6} s. These phases were assigned to recombination from two different internal sites. Based on molecular modeling studies, the authors proposed that the slower geminate processes correspond to rebinding from more internal cavities as was observed in Mb (3). To locate these internal, apolar cavities, Savino *et al.* (30) crystallized deoxyHbA under high pressure of Xe gas. Several Xe atoms were modeled into the electron density with some positions corresponding spatially to the Xe4 and Xe2 cavities in Mb. Savino *et al.* (30) proposed that these Xe binding sites map multiple ligand migration pathways from the active site to the solvent in both subunits of human HbA.

In our previous work, we attempted to shut the E7 gate in HbA by replacing the distal His with a larger Trp residue (31, 32). The bimolecular rates of CO and O₂ binding to the blocked and closed Trp(E7) conformers in HbA decreased ≥ 10 -fold in comparison to those for WT HbA, suggesting that $\geq 90\%$ of ligands enter the active site via the His(E7) gate. However, we did not explore the role of distal pocket volume and internal cavities in regulating bimolecular ligand binding. In an attempt to reconcile the discrepancy between our mutagenesis work at the E7 position and the Xe binding and theoretical work of Sottini *et al.* (28, 29) and Savino *et al.* (30), respectively, we have systematically measured the

effects of high Xe pressures and Phe and Trp substitutions at the internal B10, E11 and G8 positions on ligand binding to isolated α and β subunits and tetrameric HbA. The results indicate that in native HbA ligands are sequestered near the Fe atom after photodissociation, do not migrate into internal cavities, and escape and enter the distal pocket by the E7 gate, a pathway that appears to be universal for vertebrate myoglobins and red cell hemoglobins.

MATERIALS AND METHODS

Recombinant Hb (rHb) mutagenesis, expression and purification

The original plasmid system for expressing rHb with V1M mutations in each subunit and the bacterial strain for production with added external hemin were developed at Somatogen, Inc. (33). Mutagenesis was performed using Stratagene PCR-based "QuikChangeTM Site-Directed Mutagenesis" kit (Stratagene, La Jolla, CA, USA). Cell growth and protein expression protocols were described previously in Birukou *et al.* (31). Protein was isolated and purified according to Looker *et al.* (33). Individual Hb subunits were obtained following the procedure described in Birukou *et al.* (31). The purity of isolated Hb subunits was assessed by cellulose-acetate electrophoresis (Helena Laboratories, Beaumont, TX, USA).

Laser photolysis of Hb subunits in O₂/CO mixtures

Association rate constants for O₂ and CO binding to the mutant Hbs (k'_{O_2} and k'_{CO}) were measured using laser flash-photolysis of the stable HbCO complexes in O₂/CO mixtures ranging from ~100% O₂ to 100% CO. Photolysis was initiated by a 0.5 μ s excitation pulse generated by a Phase-R 2100B dye laser system (New Durham, NH, USA) using Rhodamine 575. The initial rapid, bimolecular phases were used to determine k'_{O_2} and k'_{CO} as described in Birukou *et al.* (31) and Salter *et al.* (25). In selected cases, the k'_{O_2} values were determined by photolysis of the HbO₂ complex.

NO binding and NO dioxygenation

Parameters for bimolecular NO binding to isolated mutant α and β subunits were obtained using a flow-flash method, in which an anaerobic solution of HbCO with no excess CO was mixed with high concentrations of NO and then immediately photolyzed to allow complete binding of NO to the transiently formed deoxyHb as described in Birukou *et al.* (31). The rate constants for NO dioxygenation by HbO₂ complexes were measured by mixing 2 μ M solutions of oxygenated forms of α and β subunits with 10 μ M solutions of NO in a modified Gibson-Durrum stopped-flow spectrophotometer D-110 (originally from Dionex Instrument, Palo Alto, CA, USA). Absorbance changes were measured at 402 nm. Experiments were conducted in 100 mM sodium phosphate, pH 7, at 20 °C. A detailed description of preparation of gas-saturated solutions of NO, O₂ and CO can be found in Birukou *et al.* (31), and the protocols for NO dioxygenation have been described previously (34, 35).

Geminate CO recombination

Time courses for geminate CO recombination within isolated native and mutant HbCO subunits were collected after excitation with a 7 ns pulse from a frequency-doubled YM600 Nd:YAG laser system (Lumonics, Inc., Billerica, MA) (25, 31). The sample was illuminated by a pulsed Xe arc lamp (model 03-102, Applied Photophysics, Inc, Leatherhead, UK) to increase the "signal-to-noise" of the absorbance traces. Transmittance was measured at 436 nm using a photomultiplier tube with a 0.9 ns response time (R-1913, Hamamatsu, Japan). 32 traces were averaged for each measurement. All measurements were performed at 20 °C in 100 mM Sodium phosphate, pH 7. Several grains of sodium dithionite were added into each cuvette for the HbCO complexes to remove residual O₂ and prevent Hb oxidation.

Xe binding experiments

The method for adding high pressures of Xe gas was adopted from Pesce *et al.* (26) and Scott *et al.* (4). Bimolecular O₂ and CO binding and geminate CO recombination to HbA tetramers and isolated subunits were measured in the presence of 0, 4 and 9 atm of Xe in a stainless steel pressure cell constructed originally by Quentin H. Gibson (4). A small amount of Hb sample (0.5–1 mL) equilibrated with 1 atm CO (1000 μM CO) or 1 atm of air (~250 μM O₂) was introduced into the pressure cell, which was sealed with a rubber septum and purged with CO or air, respectively, in advance of pressurization. For CO samples, several grains of dithionite were added into the cell before introducing the sample. Initially time courses for O₂ and CO binding were collected in the absence of Xe, either in air or pure CO, both at 1 atm pressure. Then, Xe was introduced via a three-way valve attached to the cell, allowing no gas from the original sample to escape. The solution in the cuvette was equilibrated with the Xe/CO or Xe/air mixture by extensively shaking the cuvette for several minutes. The final total pressures of the gas mixtures in the cell were 1, 5 and 10 atm. Bimolecular and geminate rebinding measurements were conducted as described above, within 10 – 20 minutes after equilibration with Xe.

RESULTS

Nanosecond CO recombination to native α and β subunits and HbA tetramers

Geminate rebinding after laser photolysis provides indirect evidence for the extent of ligand migration that occurs inside globins immediately after photolysis of the Fe-ligand bond. Depending on the reactivity of the ligand and Fe, the length of the laser pulse, and the experimental conditions, rebinding from the initial docking site of the ligand and from more distant locations within the protein can be observed. Compared to Mb where the rate of internal O₂ rebinding is moderate, ~ 10 μs⁻¹ (3), O₂ geminate recombination in HbA is very fast (>100 μs⁻¹) because of the high reactivity of the heme Fe (36) and reflects primarily ligand rebinding from the vicinity of Fe atom (37). More information about ligand migration in HbA subunits can be obtained by measuring geminate CO recombination, because the rate of Fe-CO bond formation is ~10-fold smaller than that for Fe-O₂, allowing CO migration to more distant sites. In the case of Mb, the low reactivity of the iron atom is due to constraints on in plane movement of the proximal histidine. These restrictions decrease the rate of internal CO recombination in Mb to ≤ 0.1 μs⁻¹ (38), and as a result, there is little or no geminate recombination at room temperature (≤ 5%). Thus, the effects of mutagenesis on ligand migration in Mb can only be examined under physiological conditions using O₂.

Figure 1 shows the time course for geminate CO recombination within a native human HbA tetramer. The trace is clearly biphasic, with one ultra-fast phase followed by a slower geminate rebinding process, which occurs with a half-time of 50–100 ns. The ultra-fast rebinding phase cannot readily be resolved using our 7 ns YAG laser because it decays simultaneously or even faster than the laser pulse at a rate >100 μs⁻¹. A representation of the events occurring after the laser flash is provided in Scheme 1 and based on previous interpretations of geminate rebinding in HbA subunits and Mb (4, 15, 37, 39, 40). The ultra-fast phase corresponds to ligand recombination from an initial B or first geminate state, presumably representing ligand transiently located just above the Fe atom. The existence of this initial "docking" site was previously identified in Mb (40) and suggested for hemoglobin subunits (37). The slower geminate phase represents recombination of ligands in rapid equilibrium between state B and locations C₁, C₂, etc., which are more distant from the Fe but still within or adjacent to the distal pocket.

When rebinding and escape from the B state (k_1 and k_2) are significantly faster than geminate rebinding from the C states, the mechanism can be simplified to a two-step scheme

with a single geminate intermediate, C, which represents rebinding by ligands that are in or near the distal pocket (Scheme 2). In terms of scheme 1, the rate of ligand-Fe bond formation can be expressed as $k_{\text{bond}} = k_3 k_1 / (k_1 + k_2)$.

Scheme 2 allows calculation of the rates of ligand bond formation (k_{bond}), escape from the protein, (k_{escape}) and entry (k'_{entry}) using: (a) the fitted fraction of geminate recombination, $F_{\text{gem}} = k_{\text{bond}} / (k_{\text{bond}} + k_{\text{escape}})$; (b) the observed rate of recombination, $k_{\text{gem}} = k_{\text{bond}} + k_{\text{escape}}$; and (c) the overall bimolecular association rate constant for CO rebinding from solvent, $k'_{\text{CO}} = k'_{\text{entry}} k_{\text{bond}} / (k_{\text{bond}} + k_{\text{escape}})$, which is measured on much longer time scales (15).

$$k_{\text{bond}} = k_{\text{gem}} F_{\text{gem}}; k'_{\text{entry}} = \frac{k'_{\text{CO}}}{F_{\text{gem}}}; k_{\text{escape}} = k_{\text{gem}} (1 - F_{\text{gem}})$$

Equations 1, 2, and 3.

Time courses for geminate CO rebinding to isolated α and β subunits of HbA are shown in Figure 2A, and, as with tetrameric HbA, a small ultrafast phase is seen, with roughly the same amplitude for all three proteins. In contrast, there are significant differences between the subunits on longer time scales. Fitted parameters for the α and β slow geminate phases are listed in Table 1 and agree well with previous measurements using a longer excitation pulse (37). Nanosecond geminate rebinding is faster in α than in β subunits ($20 \mu\text{s}^{-1}$ versus $7 \mu\text{s}^{-1}$, respectively), whereas the fraction of recombination is larger in β than in α subunits, 0.26 versus 0.16, respectively (Table 1).

When the subunits are present in tetramers, all the geminate parameters increase. F_{gem} becomes ~ 0.30 for both subunits due to 2 to 3-fold increases in k_{bond} (Table 1). In contrast, there is very little difference in k_{escape} values for tetramers versus isolated subunits, and Birukou *et al.* (31) showed that there is also very little difference between the k'_{entry} values for isolated versus tetrameric subunits. Thus, the increase in k_{bond} for the subunits in tetramers suggests that the Fe atom is more reactive, perhaps due to fixing the proximal heme-His(F8) complex in a staggered orientation due to interactions with partner subunits. In contrast, the F-helices in isolated subunits are probably more flexible. This interpretation is supported by the observation that the α subunits show the largest increase in k_{bond} , presumably because these subunits are almost completely monomeric at the protein concentrations used (50 – $100 \mu\text{M}$), whereas, under these conditions, isolated β subunits are primarily homo-tetrameric.

Geminate and bimolecular ligand binding to B10 mutants

Representative time courses for geminate CO recombination in α Phe(B10), β Phe(B10) and β Trp(B10) isolated subunits are shown in Figure 2B. The ultra-fast phase, reflecting ligand rebinding from the initial photodissociated B state, was observed in the time courses for each mutant subunit, but then little or no slow nanosecond recombination is observed for these variants, with the exception of β Trp(B10). The α Trp(B10) mutant is too unstable to be prepared as an isolated chain. Consequently, the hybrid α (Trp(B10)) β (WT) tetramer was used to measure parameters for the α Trp(B10) subunit. The fitted parameters for the slow nanosecond geminate phases of the B10 mutants are listed in Table 2, and F_{gem} represents the fraction of the slower geminate phase.

In α subunits, both the Phe(B10) and Trp(B10) mutations cause complete inhibition of nanosecond geminate rebinding. In β Phe(B10) subunits, the fraction of nanosecond geminate recombination is reduced to 4%. These results are consistent with the effects of Phe and TrpB10 replacements on geminate O₂ rebinding to Mb, where F_{gem} is reduced from 0.5 for wild-type Mb to 0.3 and 0.05 for the Phe and Trp(B10) mutants, respectively (3). Pronounced reduction of nanosecond geminate CO rebinding was also reported for

tetrameric Hb mutants containing Tyr(B10) and Gln(E7) in both subunits (41) and hybrid Hb tetramers containing α Phe(B10) or α Trp(B10) and allosteric mutations (42). These results demonstrate that bulky aromatic side chains at the B10 position severely hinder access of photodissociated ligands to the heme Fe atom in all three globins, decreasing k_{bond} markedly.

Surprisingly, the geminate recombination parameters for β Trp(B10) are very similar to those for WT β subunits (Table 2). The more flexible β distal pocket appears to be able to accommodate both the large Trp(B10) side chain and the bound ligand, and rebinding from the C geminate state is not inhibited by the indole side chain, which appears to have moved away from the active site and is unable to swing back over the Fe atom until the ligand has left the pocket. The biphasic character of bimolecular CO rebinding to this mutant suggests that the TrpB10 side chain in β subunits can occupy at least two distinct conformations, one with the indole ring greatly hindering ligand binding as is observed for α Trp(B10), and one where the B10 side chain is pointing away from the Fe atom (Table 2).

Space-filling mutations at the B10 position also dramatically affect bimolecular ligand binding, particularly for α subunits. The CO association rate constant, k'_{CO} , decreases 160 and 1600-fold for the α Phe(B10) and α Trp(B10) mutants, respectively, compared to that for the WT α subunit. Similar trends are observed for O₂ and NO binding (Table 2, second and third rows). The large differences between the absolute values of k'_{NO} , k'_{O_2} , and k'_{CO} are due to intrinsic differences in the ligand reactivities with Fe (NO > O₂ >> CO), with Fe-ligand bond formation being rate-limiting for CO binding and ligand entry into the distal pocket being rate limiting for NO binding (34, 44). O₂ association is regulated by a combination of these processes. The dramatic inhibition of CO binding to the α Phe(B10) and α Trp(B10) mutants is caused by severe hindrance of access to the Fe atom by the large phenyl and indole rings. The smaller 6- and 30-fold decreases in k'_{NO} for the α Phe(B10) and α Trp(B10) mutants, respectively, reflect the decrease in size of the distal volume for the initial non-covalent capture of the ligand molecule. The decreases in k'_{O_2} are intermediate between those for CO and NO, supporting the idea that both ligand entry and ligand-Fe bond formation limit O₂ association.

Bimolecular binding to the β (B10) mutants is more complex due to the appearance of an initial fast phase (~50% of the amplitude) with a rate similar to that of WT β subunits and an ultra-slow phase similar to that seen for the α (B10) mutants (Table 2). The faster phase almost certainly reflects an alternative, less hindered conformation of the large phenyl and indole B10 side chains. The presence of conformational heterogeneity in the β Phe(B10) and Trp(B10) mutants of Hb was previously noticed in NMR studies by Wiltrot *et al.* (45). The crystal structures of HbA alkyl isocyanide complexes show that the Leu(B10) side chain in β subunits is flexible and can move away from large bound ligand molecules toward Leu(B13), whereas in α subunits the Leu(B10) side chain is held in place by the larger Met(B13) side chain (34). This flexibility in the β subunits also appears to occur in Phe(B10) and Trp(B10) mutants, as judged by the presence of two bimolecular phases and the lack of effect of the large aromatic side chains on the fast bimolecular phases for the binding of all three ligands (Table 2).

The rate constants for slow bimolecular ligand binding to β Trp(B10) are identical to those for α Trp(B10) subunits, suggesting that about 50% of the β Trp(B10) indole side chains are located directly above the heme Fe atom. When rate parameters for ligand binding to the β Phe(B10) and Trp(B10) mutants were estimated for subunits within mutant/WT hybrid tetramers, only the ultra slow phases could be resolved from the WT subunit binding phases. As shown in Table 2, the k'_{CO} and k'_{O_2} values for the mutant subunits in tetramers are very similar to those determined for the slow bimolecular phases observed with isolated subunits.

As is the case for simple NO binding to deoxyHb, bimolecular ligand entry into the distal pocket is also the rate limiting step for NO dioxygenation by HbO₂ complexes, which is measured by rapidly mixing solutions of αO₂ or βO₂ with varying [NO] (34). Thus, k'_{NOD} as well as k'_{NO} can be used to verify the values of k'_{entry} computed from overall and geminate CO binding parameters. As expected NO dioxygenation is significantly inhibited in α Phe(B10), α Trp(B10), and β Trp(B10) subunits (Table 2), whereas k'_{NOD} and k'_{NO} are little affected or increase slightly for the βPhe(B10) mutant as was observed previously (34).

Geminate and bimolecular ligand binding to E11 mutants

Time courses for geminate CO recombination to Phe and Trp (E11) mutants of the α and β subunits are shown in Figure 2C. There is no distinct ultrafast geminate phase for these variants. Fitted geminate parameters and calculated rates of bond formation and escape are listed in Table 3. Unlike the position B10 substitutions, the Phe and Trp (E11) mutations markedly increase F_{gem,CO} in HbA, from 0.16 to 0.70 in α mutants and from 0.26 to 0.90 in β mutants. Analogous effects were reported for Phe and Trp (E11) mutants of Mb, where F_{gem,O2} increased from 0.50 in WT protein to ≥ 0.90 in the E11 aromatic amino acid variants.

The increases in F_{gem} for the Phe(E11) mutants are due primarily to 10- and 20-fold increases in k_{bond} for the α and β subunits, respectively. The analysis of the Hb Trp(E11) mutants is complicated by the presence of two slow nanosecond geminate phases. However, regardless of the interpretation of these two phases, it is clear that the increase in geminate recombination is due to markedly increased k_{bond} values. To simplify the analysis, we assumed that the two Trp(E11) phases for each subunit represent distinct non-interconverting conformations, fitted the time courses to two independent exponential expressions, and analyzed each phase in terms of Equations 1–3. In the α Trp(E11), k_{bond} increases 2- to 5-fold and in β Trp(E11), k_{bond} increases 10-fold for the larger phase, whereas the parameters for the smaller phase are similar to those for the WT β subunit. Variations in k_{escape} for the E11 mutants are small, ranging from ~ 2-fold increases to 50% decreases (Table 3).

The effects of the E11 mutations are due to loss of steric hindrance by the γ2 methyl group of Val(E11) and confinement of the ligand close to the iron atom by the large aromatic side chains, both of which increases k_{bond}. Crystal structures of the Mb TrpE11 (15) and PheE11 (44) mutants verify this interpretation and show both loss of steric hindrance near the Fe atom and a decrease in distal pocket volume when compared to WT Mb. In both HbA and Mb, these effects result in greater rates and extents of geminate recombination in the E11 mutants.

The rate constants for bimolecular CO binding to the HbA Phe(E11) mutants are not dramatically different from the WT values, but 2 to 4-fold decreases in k'_{NO} and k'_{O2} are observed. Release of steric hindrance at the Fe atom as a result of the Val(E11) to Phe substitution increases k_{bond}, but this rate enhancement is offset by reduction in the capture volume for ligands in the back of the distal cavity where the phenyl ring resides. These effects roughly compensate each other, accounting for the lack of change in k'_{CO}. However, in the case of NO binding, the rate-limiting step is ligand entry, which decreases in the presence of Phe(E11) due to loss of distal pocket volume.

Both α Trp(E11) and β Trp(E11) mutants reveal biphasic bimolecular ligand binding. In α Trp(E11), the fast phase parameters for bimolecular CO, O₂ and NO binding are identical to those for the α Phe(E11) mutant, suggesting that Trp residue has a conformation similar to that of the αPhe(E11) side chain. The slower binding phase probably represents an α Trp(E11) conformer in which the indole ring is filling more of the distal pocket cavity,

greatly inhibiting ligand entry into the active site. Similar conclusions can be drawn for the slow phase of bimolecular ligand binding to β Trp(E11). The values of k'_{NOD} for the oxygenated complexes of α Phe(E11) and α Trp(E11) mutants are similar to those for the WT subunits suggesting that the more open conformations are preferred when O_2 is bound. However, significant decreases (3 to 5-fold) in k'_{NOD} are observed for the isolated or tetrameric β Phe(E11) and β Trp(E11) subunits.

Geminate and bimolecular ligand binding to G8 mutants

Phe and Trp substitutions at the G8 position do not produce significant changes in the rate and extent of slow, nanosecond geminate CO recombination from the C state in isolated Hb subunits (Figure 2D, Table 4). In α subunits, k_{bond} decreased only marginally for the Phe(G8) and Trp(G8) mutants, and similar 30% decreases were observed for k_{escape} . β Phe(G8) showed the largest change in F_{gem} , which decreased 2-fold due to a decrease in k_{bond} from 1.9 to $0.6 \mu\text{s}^{-1}$ for the WT and mutant subunits, respectively. Both k_{bond} and k_{escape} decreased ~2-fold, for β Trp(G8), leaving F_{gem} unchanged. These latter changes suggest that the distal pocket of the β subunits is slightly expanded by the Trp(G8) indole side chain, allowing the ligand to linger in the distal pocket without affecting the probability of recombining or escaping. In contrast, the Phe(G8) and Trp(G8) substitutions increase both k_{bond} and k_{escape} in Mb, which is consistent with a decreased distal pocket volume (3).

The HbA G8 mutants do cause measurable changes in the overall bimolecular kinetic parameters (Table 4). Decreases in k'_{CO} and k'_{O_2} with increasing the size of the G8 residue are observed for both subunits. However, the k'_{NO} , k'_{NOD} , and the calculated k'_{entry} values remain relatively unchanged (≤ 2 -fold). Only the β Trp(G8) mutant shows large (≥ 5 -fold) decreases in the bimolecular rate constants for the binding of all three gases, ligand entry, and NO dioxygenation. Thus, only in β subunits does the Leu(G8) to Trp mutation cause a functionally measurable decrease in the ligand capture volume.

Effects of Xe pressure on ligand binding to HbA and its subunits

Time courses for geminate CO recombination to isolated WT Hb subunits under high pressures of Xe gas are shown in Figure 3, and the resultant kinetic parameters are listed in Table 5. Non-specific pressure effects on ligand binding to globins have been ruled out by previous work (4, 5, 26). Small increases in F_{gem} are detected for isolated native α CO subunits when the Xe partial pressure is increased to 9 atm and are due to an $\sim 50\%$ increase of k_{bond} from 3.1 to $4.8 \mu\text{s}^{-1}$. The values of k_{escape} , k'_{O_2} , and k'_{CO} for isolated α subunits show no statistically significant changes. Time courses for geminate CO rebinding to β subunits at high Xe pressures are shown in Figure 3B. Again, F_{gem} increases slightly due to a small increase in k_{bond} , and, in this case, the bimolecular rate constants for ligand binding do decrease ~20% at high pressures of Xe, but this change is probably not statistically significant (Table 5). Thus, filling internal globin cavities with Xe has very little effect on either geminate or bimolecular ligand binding in the α and β subunits in contrast to the space filling Phe and Trp mutations at the B10 and E11 helical positions.

The kinetic parameters for internal CO rebinding within intact HbA tetramers are also little affected by Xe pressure, even though the fraction of geminate recombination is higher under all conditions (Table 6). Again, a small increase in F_{gem} is observed for α subunits at 9 atm Xe due to a 60% increase in k_{bond} with little or no change in k_{escape} . However, the key result in Table 6 is that Xe binding has little or no effect on ligand binding to tetramers as well as monomers.

To assess the influence of Xe atoms on ligand binding to T-state HbA, we measured CO rebinding to Hb tetramers after full photolysis, which allows the protein to switch to the low

affinity T state quaternary conformation. The time courses at varying Xe pressures are virtually indistinguishable from those in its absence (not shown). The rate constants for CO binding to T-state HbA (k'_{TCO}) were determined by analyzing the slow, accelerating phases of each full photolysis trace. No changes in k'_{TCO} were detected upon addition of Xe (Table 6).

DISCUSSION

Structural interpretations

The crystal structures of recombinant HbA variants containing B10, E11, and G8 mutations were determined previously following procedures described in (46), and the coordinates were deposited in the Protein Data Bank by E. A. Brucker in 2002 (1O1I – 1O1P). The most relevant structures for interpreting our kinetic studies include the deoxy forms of $\alpha_1(\text{Met(NA1)}/\text{Trp(B10)})-(\text{Gly})_3-\alpha_2(\text{Trp(B10)}):\beta(\text{Met(NA1)})$ (1O1N), $\alpha_1(\text{Met(NA1)}/\text{Phe(B10)}/\text{Gln(E7)})-\text{Gly}-\alpha_2-(\text{Phe(B10)}/\text{Gln(E7)}):\beta(\text{Met(NA1)}/\text{Trp(G8)})$ (1O1J), and $\alpha_1(\text{Met(NA1)}/\text{Phe(B10)}/\text{Gln(E7)})-(\text{Gly})_3-\alpha_2(\text{Phe(B10)}/\text{Gln(E7)}):\beta(\text{Met(NA1)}/\text{Trp(E11)})$ (1O1M), and the cyanomet form of $\alpha_1(\text{Met(NA1)}/\text{Phe(B10)}/\text{Gln(E7)})-\text{Gly}-\alpha_2-(\text{Phe(B10)}/\text{Gln(E7)}):\beta(\text{Met(NA1)}/\text{Trp(G8)})$ (1O1I). One to three Gly residues were introduced between α_1 and α_2 subunits in these recombinant Hbs to prevent dissociation into dimers as part of an effort to design a safe and effective Hb-based oxygen carrier (33). The Met(NA1) mutation is not present in the α_2 subunit domain because the α_1 and α_2 subunits were expressed as a single di- α polypeptide.

The structures of the distal pockets of deoxy- α Trp(B10), deoxy- α Phe(B10)/Gln(E7), deoxy- β Trp(E11) and cyanomet- β Trp(G8) subunits in WT/mutant hybrid tetramers of recombinant HbA are presented in Figure 4. *Panels A* and *B* show clearly that the immediate vicinity of the Fe atom is restricted by large aromatic side chains at the B10 position in α chains. The distances from Fe to the closest edges of the α Phe(B10) and α Trp(B10) side chains are 5.5 Å and 4.8 Å, respectively. In native α subunits, the distance from Fe to the C δ 2 methyl of Leu(B10) is 7.4 Å. In WT α subunits, the Leu(B10) and His(E7) side chains are far enough away from the Fe and flexible enough to allow up to 30% geminate CO recombination. In contrast, the aromatic rings of α Phe(B10) and Trp(B10) side chains sterically hinder the formation of the first geminate state (state B in Scheme 1), push the ligands out of the distal pocket toward either solvent or the protein interior, and almost completely abolish nanosecond geminate rebinding. The conformations of the α Phe(B10) and Trp(B10) side chains shown in Figure 4 are almost identical to those of Phe(B10) and Trp(B10) in Mb mutants (15, 44).

When Trp is substituted for Val(E11) in β subunits, two significant structural changes occur (Figure 4C). First, the indole side chain fills the accessible space in the back of the distal pocket markedly reducing the capture volume in the distal pocket. Second, loss of the γ 2 methyl group of Val(E11) removes steric restriction adjacent to the Fe atom, enhancing the rate of internal bond formation. These structural features explain the dramatic increases in the fractions and rates of CO geminate recombination in all four Hb Phe(E11) and Trp(E11) mutants and in the corresponding Mb E11 variants (15, 44).

Neither the α or β Trp(G8) mutations cause any significant effects on CO geminate recombination, suggesting that this amino acid is not part of a ligand migration pathway toward cavities in the protein interior. In contrast, the Mb Ile(G8) to Trp mutation does cause an almost complete loss of the slow microsecond phase of O₂ geminate recombination that is associated with ligand movement into and return from the Xe1 and Xe4 sites (3, 15). Structural differences between β Trp(G8) subunits and Mb Trp(G8) are shown in Figure 5. The structure of the WT β HbO₂ distal pocket (blue) is superimposed on the model for the

cyanomet- β Trp(G8) mutant (white) in *panel A*. In WT β subunits, the side chain of Phe(E15) is close to the pyrrole B ring, is parallel to the heme plane, and fills an area spatially similar to the Xe4 cavity in Mb (brown sphere above the heme plane in Figure 5A). In the β Trp(G8) mutant, the Phe(E15) side chain has rotated $\sim 90^\circ$ away from the heme to accommodate the bulky G8 indole group, which occupies part of the same space that the E15 phenyl ring fills in the β WT distal pocket. Thus, the net change in accessible distal pocket volume caused by the Leu(G8) to Trp mutation is relatively small, and there is no direct route to the protein interior in either the β WT or Trp(G8) variants.

In Mb, the Trp(G8) side chain does not displace any distal pocket side chains and, instead, assumes a conformation in which the indole ring is located above the edge of the pyrrole B ring, reduces the size of the capture volume, and blocks access to the Xe4 cavity (Figure 5B). Thus, in Mb, Trp(G8) accelerates bond formation by sequestering ligands closer to the Fe atom and blocking ligand access to the Xe1 and Xe4 binding sites (3, 15).

In the deoxy- β Trp(G8) distal pocket (Figure 6), the conformation of the G8 indole side chain is similar to that in cyanomet-form, however, a water molecule is coordinated to the pyrrole nitrogen of the indole ring and the carbonyl O atoms of Gly(B6) and Gly(E8). The distances between the water and these atoms of Trp(G8), Gly(B6) and Gly(E8) (3.2 Å, 2.8 Å and 3.1 Å, respectively) indicate the formation of strong hydrogen bonds. As a result, the distal capture volume in the equilibrium form of deoxy β Trp(G8) is significantly smaller than that in WT β subunits, resulting in a 4-fold decrease in k' entry (Table 4). However, this water molecule is not present in the initial liganded state of β Trp(G8) and has no effect on geminate rebinding. This internalization of a water molecule in the equilibrium structure of the mutant deoxy- β Trp(G8) subunit explains the apparent discrepancy between the 4-fold decrease k' entry and the lack of an effect on geminate recombination, which occurs before water can enter the distal pocket (Table 4).

Ligand trapping in the distal pocket

The equilibrium constant for ligand entry can be computed as $K_{\text{entry}} = k'_{\text{entry}}/k_{\text{escape}}$ to quantify the non-covalent ligand capture efficiency of the distal pocket. This constant depends primarily on the volume available to ligands in or near the active site, which serves to retain the captured ligand until it binds to the heme Fe. For native α and β subunits these values are 2.0 ± 0.2 and $8.4 \pm 2.0 \text{ M}^{-1}$, respectively, based on our data and previous work (31, 47). The presence of a distal pocket water hydrogen bonded to His(E7) in WT α subunits and the lack of flexibility of Leu(B10) contributes to its smaller K_{entry} value compared to β subunits (Figure 6, (34, 48, 49)). Significant decreases in K_{entry} occur for the Phe and Trp B10 and E11 mutants, with the Trp replacements showing 5 to 10-fold decreases (Tables 2–3). The Trp(G8) replacement has no effect on K_{entry} in α subunits (Table 4, Figure 7), whereas this mutation causes 3 to 4-fold decreases in K_{entry} in Mb and β subunits. The decrease in capture volume in Mb is due to the orientation of the G8 indole side chain over the heme group, which blocks access to the Xe4 cavity (Figure 5B). The decrease in K_{entry} for deoxy β Trp(G8) is due both primarily to the presence of a water molecule hydrogen bonded to the indole N atom (Figure 6).

The results in Figure 7 also show that the addition of Xe has little effect on the accessibility of the non-covalent capture volume in either Mb or the α subunits of HbA. The only statistically significant effect is observed for β subunits, where K_{entry} decreased ≤ 2 -fold in the present of 9 atm of Xe gas (Table 5, Figure 7). This decrease suggests that a small fraction of Xe atoms can penetrate into the β distal pocket and reduce the volume of the non-covalent binding site. In contrast, the α distal pocket appears to be too small to accommodate a Xe atom.

Ultra-fast phase of geminate recombination and secondary sites in HbA

Geminate O₂ recombination in Mb is multi-exponential with a fast, nanosecond phase reflecting ligand association from the distal pocket and adjacent Xe4 cavity and slower, microsecond phases representing ligand rebinding from the more distant Xe1 site (3, 4, 15, 50). Sottini *et al.* (28, 29) reported multiple geminate phases in human HbA similar to those shown in Figures 1–3 (28, 29). Based on the mechanism for geminate O₂ recombination to Mb, these authors assigned the slower phase to ligand rebinding from remote sites, distinct from the distal pocket. The faster phase was assigned to ligand recombination from within the distal pocket. In contrast, our results suggest that there are no remote, secondary docking sites in HbA analogous to those seen in Mb. We assign the slower nanosecond phase for CO geminate recombination in HbA to ligand rebinding from within the distal pocket or sites closely adjacent to it. The ultra-fast phase was assigned to rebinding from an initial geminate state, where the ligand is transiently very near the Fe atom (Scheme 1, state B). Our interpretation is based on the following arguments.

First, the slower phase for CO geminate recombination still occurs with the same amplitude in the presence of high pressures of Xe gas in both isolated and tetrameric HbA subunits (Figure 3). In contrast, high Xe pressures eliminate the slow O₂ recombination phase in Mb due to occupation of secondary Xe4 and Xe1 sites. Second, the slower CO recombination phase in the HbA subunits occurs with a half-time of ~50 to 100 ns which is similar to the faster O₂ recombination phase seen in WT Mb and contrasts with the slow CO and O₂ geminate phases in WT Mb, which have half-times \approx 1–2 μ s. Third, the pathways leading to the proposed Xe binding sites in HbA ((28–30), Figure 8) should be sterically hindered by the space-filling E11 mutations, especially by the Trp replacements, which would be expected to decrease the fraction of the slow geminate recombination and increase the fraction of the fast phase. In our experiments, however, the slow phases for CO geminate recombination do not disappear and the ultra-fast phases are not observed at all in the geminate time courses for the α and β E11 mutants (Figure 2C). The absence of the ultra-fast phase for the internal CO rebinding in E11 mutants of HbA suggests that the naturally occurring Val(E11) γ 2 methyl group is the structural barrier between states B and C in Scheme 1.

Ligand migration via alternative routes in HbA

Figure 8 shows the crystal structures of the α and β Hb subunits with bound Xe atoms as determined by Savino *et al.* (30). These authors proposed that the cavities occupied by Xe atoms transiently open and form a channel within the protein matrix that guides ligand migration from solvent to the distal pocket and *vice versa*. One of these tunnels is more pronounced in β subunits, contains a string of well-ordered waters and Xe atoms, and appears to identify a potential migratory pathway that is analogous to the apolar tunnel in *Cerebratulus lacteus* mini-Hb (25, 26).

This proposed tunnel in β subunits can be blocked by mutating Val(E11) to Trp (see Figures 4C and 8B). In β Trp(E11), the indole ring of the Trp is located in the space above the B ring of the porphyrin. The Xe2 atom occupies that same position in the structure of β WT at high gas pressures (Figure 8B). The dramatic increase in the fraction of recombination due to presence of Trp(E11) (Table 3, Figure 2C) could be interpreted as supporting the alternative migration route through the Xe2 cavity. However, the calculated rates of escape do not decrease in the Trp(E11) mutants but instead increase 2-fold (Table 3). The observed increases in the fractions of recombination in the Hb Trp(E11) mutants are due almost exclusively to markedly larger rates of ligand-Fe bond formation (k_{bond} in Table 3) and not to slow rates of escape. More importantly, Xe binding does not show any significant inhibition of ligand entry or escape (Tables 5 and 6).

The absence of effects of Xe on ligand recombination in HbA is not a surprise. In Mb, increasing Xe partial pressure does not change the fraction of CO recombination, which is inherently very small (~0.05) (26). In the case of geminate O₂ rebinding to Mb, the total amount of recombination also stays unchanged upon addition of up to ~10 atm of Xe; however, the slow μ s phase of the geminate reaction does disappear because ligands can no longer enter the Xe1 and Xe4 sites (3, 4). The lack of effect on the overall fraction of geminate recombination suggests strongly that, even though ligands do visit the Xe binding sites in the Mb protein matrix, these cavities do not serve as ports of entry or escape. In *Scapharca inaequivalvis* HbI dimers, Xe binding also has no effect the fraction of ligand escape even though MD simulations suggest that ligands migrate through Xe binding cavities and into solvent (23). Only in the mini-Hb from *Cerebratulus lacteus* does Xe binding significantly increase the fraction of geminate CO recombination (increasing F_{gem} from 0.05 to ~0.30) and decrease the rate of ligand entry into the protein, confirming that its apolar tunnel is the major route for ligand entry and escape (26).

A key remaining question is whether the His(E7) pathway also applies in T-state deoxyhemoglobin or is affected by the R to T quaternary transition. At present, there is little evidence suggesting that the pathways for ligand movement into the active sites of the α and β subunits are altered markedly by the quaternary transition. First, the conformations of the amino acids in and near the His(E7) gate are not dramatically altered comparing high resolution deoxyHbA and oxyHbA structures, except for the inward movement of the distal histidine when the ligand is not present and some movement of the E-helix across the distal face of the heme (49). Second, this gate is exposed to solvent and far from both the $\alpha 1\beta 1$ and $\alpha 1\beta 2$ interfaces (49). Third, Cassoly and Gibson (51) have shown that the bimolecular rate constant for NO association is roughly the same for first and last steps in ligand binding, and we have observed the same result (52). Because of its high reactivity, the limiting step for NO binding is diffusion into the active site. Thus, there is very little change in k' entry between the R and T states, and probably the same pathway applies in each case. However, a more detailed analysis of bimolecular rate constants for the T-state forms of mutant Hb tetramers is needed to verify this conclusion.

CONCLUSION

Our results for space filling mutations and Xe binding, combined with previous kinetic data for His(E7) mutations (31, 32), suggest strongly that the “baseball glove” model for ligand binding, originally proposed for sperm whale Mb (3), also applies to the α and β subunits of human HbA, either when isolated or present in R-state tetramers. Reducing the volume of the non-covalent binding site in both subunits by Phe or Trp B10 and E11 mutations decreases the ability of hemoglobin to retain captured ligands for bond formation with the Fe atom. The small internal cavities, analogous to the Xe pockets in Mb, do not appear to host ligands, even transiently during nanosecond laser flash photolysis experiments. In both subunits of HbA, the fast and slow phases of geminate recombination appear to represent rebinding from an initial transient geminate state formed immediately after ligand photodissociation and then from more interior regions in or very near the distal pocket, respectively. The system of Xe-binding sites observed in crystal structures of HbA do not appear to be part of a major pathway for ligand migration because filling these cavities with Xe gas does not significantly affect the rates of ligand escape or bimolecular entry.

Abbreviations

Hb	hemoglobin
----	------------

α and β	subunits of adult human hemoglobin (HbA), which can be isolated biochemically or present in intact heterotetramers or $\alpha\beta$ dimers
Mb	myoglobin
WT	wild-type
NOD	NO dioxygenation
k'_X	association rate constant for ligand X
k_X	dissociation rate for ligand X
F_{gem}	fraction of geminate recombination
k_{gem}	rate of geminate recombination
k_{bond}	rate of internal bond formation
k_{escape}	rate of ligand escape from the protein
k'_{entry}	rate of ligand entry into distal pocket
K_{entry}	equilibrium constant for ligand capture in non-covalent binding site calculated as $k'_{\text{entry}}/k_{\text{escape}}$
Nd	YAG, neodymium-doped yttrium aluminium garnet
rmsd	root mean square deviation

Acknowledgments

We would like to acknowledge Dr. Eric A. Brucker for his substantial effort in determining and depositing the structures of large numbers of genetically crosslinked, recombinant hemoglobins when he was a Research Scientist at Somatogen, Inc. and later Baxter Hemoglobin Therapeutics in Boulder, CO. As shown in Figures 4–6 and 8, his work was crucial for interpreting the effects of the B10, E11, and G8 mutations on the kinetics of both bimolecular and geminate ligand binding. He also read the manuscript and, along with Dr. Mallory Salter and Dr. Jayashree Soman, made valuable suggestions for improving the text and figures.

REFERENCES

1. Schoenborn BP, Watson HC, Kendrew JC. Binding of xenon to sperm whale myoglobin. *Nature*. 1965; 207:28–30. [PubMed: 5893727]
2. Tilton RF Jr, Kuntz ID Jr, Petsko GA. Cavities in proteins: Structure of a metmyoglobin-xenon complex solved to 1.9 Å. *Biochemistry*. 1984; 23:2849–2857. [PubMed: 6466620]
3. Scott EE, Gibson QH, Olson JS. Mapping the pathways for O₂ entry into and exit from myoglobin. *J Biol Chem*. 2001; 276:5177–5188. [PubMed: 11018046]
4. Scott EE, Gibson QH. Ligand migration in sperm whale myoglobin. *Biochemistry*. 1997; 36:11909–11917. [PubMed: 9305984]
5. Tetreau C, Blouquit Y, Novikov E, Quiniou E, Lavalette D. Competition with xenon elicits ligand migration and escape pathways in myoglobin. *Biophys J*. 2004; 86:435–447. [PubMed: 14695286]
6. Radding W, Phillips GN Jr. Kinetic proofreading by the cavity system of myoglobin: protection from poisoning. *Bioessays*. 2004; 26:422–433. [PubMed: 15057940]
7. Ostermann A, Waschippy R, Parak FG, Nienhaus GU. Ligand binding and conformational motions in myoglobin. *Nature*. 2000; 404:205–208. [PubMed: 10724176]
8. McNaughton L, Hernandez G, LeMaster DM. Equilibrium O₂ distribution in the Zn²⁺-protoporphyrin IX deoxymyoglobin mimic: application to oxygen migration pathway analysis. *J Am Chem Soc*. 2003; 125:3813–3820. [PubMed: 12656614]
9. Case DA, Karplus M. Dynamics of ligand binding to heme proteins. *J Mol Biol*. 1979; 132:343–368. [PubMed: 533895]

10. Elber R, Karplus M. Enhanced sampling in molecular dynamics: use of the time dependent Hartree approximation for simulation of carbon monoxide diffusion through myoglobin. *J. Am. Chem. Soc.* 1990; 112:9161–9175.
11. Cohen J, Schulten K. O₂ migration pathways are not conserved across proteins of a similar fold. *Biophys J.* 2007; 93:3591–3600. [PubMed: 17693478]
12. Cohen J, Olsen KW, Schulten K. Finding gas migration pathways in proteins using implicit ligand sampling. *Methods Enzymol.* 2008; 437:439–457. [PubMed: 18433641]
13. Elber R, Gibson QH. Toward quantitative simulations of carbon monoxide escape pathways in myoglobin. *J Phys Chem B.* 2008; 112:6147–6154. [PubMed: 18205346]
14. Ruscio JZ, Kumar D, Shukla M, Prisant MG, Murali TM, Onufriev AV. Atomic level computational identification of ligand migration pathways between solvent and binding site in myoglobin. *Proc Natl Acad Sci U S A.* 2008; 105:9204–9209. [PubMed: 18599444]
15. Olson JS, Soman J, Phillips GN Jr. Ligand pathways in myoglobin: a review of Trp cavity mutations. *IUBMB Life.* 2007; 59:552–562. [PubMed: 17701550]
16. Morikis D, Champion PM, Springer BA, Sligar SG. Resonance raman investigations of site-directed mutants of myoglobin: effects of distal histidine replacement. *Biochemistry.* 1989; 28:4791–4800. [PubMed: 2765511]
17. Rohlfs RJ, Mathews AJ, Carver TE, Olson JS, Springer BA, Egeberg KD, Sligar SG. The effects of amino acid substitution at position E7 (residue 64) on the kinetics of ligand binding to sperm whale myoglobin. *J Biol Chem.* 1990; 265:3168–3176. [PubMed: 2303446]
18. Yang F, Phillips GN Jr. Crystal structures of CO-, deoxy- and met-myoglobins at various pH values. *J Mol Biol.* 1996; 256:762–774. [PubMed: 8642596]
19. Tian WD, Sage JT, Champion PM. Investigations of ligand association and dissociation rates in the "open" and "closed" states of myoglobin. *J Mol Biol.* 1993; 233:155–166. [PubMed: 8377182]
20. Tian WD, Sage JT, Champion PM, Chien E, Sligar SG. Probing heme protein conformational equilibration rates with kinetic selection. *Biochemistry.* 1996; 35:3487–3502. [PubMed: 8639499]
21. Lai HH, Li T, Lyons DS, Phillips GN Jr, Olson JS, Gibson QH. Phe-46(CD4) orients the distal histidine for hydrogen bonding to bound ligands in sperm whale myoglobin. *Proteins.* 1995; 22:322–339. [PubMed: 7479707]
22. Nienhaus K, Knapp JE, Palladino P, Royer WE Jr, Nienhaus GU. Ligand migration and binding in the dimeric hemoglobin of *Scapharca inaequivalvis*. *Biochemistry.* 2007; 46:14018–14031. [PubMed: 18001141]
23. Knapp JE, Pahl R, Cohen J, Nichols JC, Schulten K, Gibson QH, Srager V, Royer WE Jr. Ligand migration and cavities within *Scapharca* Dimeric HbI: studies by time-resolved crystallography, Xe binding, and computational analysis. *Structure.* 2009; 17:1494–1504. [PubMed: 19913484]
24. Boechi L, Marti MA, Milani M, Bolognesi M, Luque FJ, Estrin DA. Structural determinants of ligand migration in *Mycobacterium tuberculosis* truncated hemoglobin O. *Proteins.* 2008; 73:372–379. [PubMed: 18433052]
25. Salter MD, Nienhaus K, Nienhaus GU, Dewilde S, Moens L, Pesce A, Nardini M, Bolognesi M, Olson JS. The apolar channel in *Cerebratulus lacteus* hemoglobin is the route for O₂ entry and exit. *J Biol Chem.* 2008; 283:35689–35702. [PubMed: 18840607]
26. Pesce A, Nardini M, Dewilde S, Capece L, Marti MA, Congia S, Salter MD, Blouin GC, Estrin DA, Ascenzi P, Moens L, Bolognesi M, Olson JS. Ligand migration in the apolar tunnel of *cerebratulus lacteus* mini-hemoglobin. *J Biol Chem.* 2011; 286:5347–5358. [PubMed: 21147768]
27. Adachi S, Park SY, Tame JR, Shiro Y, Shibayama N. Direct observation of photolysis-induced tertiary structural changes in hemoglobin. *Proc Natl Acad Sci U S A.* 2003; 100:7039–7044. [PubMed: 12773618]
28. Sottini S, Abbruzzetti S, Spyrosakis F, Bettati S, Ronda L, Mozzarelli A, Viappiani C. Geminate rebinding in R-state hemoglobin: kinetic and computational evidence for multiple hydrophobic pockets. *J Am Chem Soc.* 2005; 127:17427–17432. [PubMed: 16332093]
29. Sottini S, Abbruzzetti S, Viappiani C, Bettati S, Ronda L, Mozzarelli A. Evidence for two geminate rebinding states following laser photolysis of R state hemoglobin encapsulated in wet silica gels. *J Phys Chem B.* 2005; 109:11411–11413. [PubMed: 16852394]

30. Savino C, Miele AE, Draghi F, Johnson KA, Sciara G, Brunori M, Vallone B. Pattern of cavities in globins: the case of human hemoglobin. *Biopolymers*. 2009; 91:1097–1107. [PubMed: 19365817]
31. Birukou I, Schweers RL, Olson JS. Distal histidine stabilizes bound O₂ and acts as a gate for ligand entry in both subunits of adult human hemoglobin. *J Biol Chem*. 2010; 285:8840–8854. [PubMed: 20080971]
32. Birukou I, Soman J, Olson JS. Blocking the gate to ligand entry in human hemoglobin. *J Biol Chem*. 2011; 286:10515–10529. [PubMed: 21193395]
33. Looker D, Mathews AJ, Neway JO, Stetler GL. Expression of recombinant human hemoglobin in *Escherichia coli*. *Methods Enzymol*. 1994; 231:364–374. [PubMed: 8041263]
34. Eich RF, Li T, Lemon DD, Doherty DH, Curry SR, Aitken JF, Mathews AJ, Johnson KA, Smith RD, Phillips GN Jr, Olson JS. Mechanism of NO-induced oxidation of myoglobin and hemoglobin. *Biochemistry*. 1996; 35:6976–6983. [PubMed: 8679521]
35. Olson JS, Foley EW, Rogge C, Tsai AL, Doyle MP, Lemon DD. No scavenging and the hypertensive effect of hemoglobin-based blood substitutes. *Free Radic Biol Med*. 2004; 36:685–697. [PubMed: 14990349]
36. Draghi F, Miele AE, Travaglini-Allocatelli C, Vallone B, Brunori M, Gibson QH, Olson JS. Controlling ligand binding in myoglobin by mutagenesis. *J Biol Chem*. 2002; 277:7509–7519. [PubMed: 11744723]
37. Olson JS, Rohlfs RJ, Gibson QH. Ligand recombination to the alpha and beta subunits of human hemoglobin. *J Biol Chem*. 1987; 262:12930–12938. [PubMed: 3654596]
38. Olson JS, Phillips GN Jr. Kinetic pathways and barriers for ligand binding to myoglobin. *J Biol Chem*. 1996; 271:17593–17596. [PubMed: 8698688]
39. Jongeward KA, Magde D, Taube DJ, Marsters JC, Traylor TG, Sharma VS. Picosecond and nanosecond geminate recombination of myoglobin with CO, O₂, NO, and isocyanides. *J Amer Chem Soc*. 1988; 110:380–387.
40. Carver TE, Rohlfs RJ, Olson JS, Gibson QH, Blackmore RS, Springer BA, Sligar SG. Analysis of the kinetic barriers for ligand binding to sperm whale myoglobin using site-directed mutagenesis and laser photolysis techniques. *J Biol Chem*. 1990; 265:20007–20020. [PubMed: 2246277]
41. Miele AE, Draghi F, Arcovito A, Bellelli A, Brunori M, Travaglini-Allocatelli C, Vallone B. Control of heme reactivity by diffusion: structural basis and functional characterization in hemoglobin mutants. *Biochemistry*. 2001; 40:14449–14458. [PubMed: 11724557]
42. Maillett DH, Simplaceanu V, Shen TJ, Ho NT, Olson JS, Ho C. Interfacial and distal-heme pocket mutations exhibit additive effects on the structure and function of hemoglobin. *Biochemistry*. 2008; 47:10551–10563. [PubMed: 18788751]
43. Maillett, DH. Biochemistry and Cell Biology. Houston: Rice University; 2003. Engineering Hemoglobins and Myoglobins for Efficient O₂ Transport.
44. Quillin ML, Li T, Olson JS, Phillips GN Jr, Dou Y, Ikeda-Saito M, Regan R, Carlson M, Gibson QH, Li H, et al. Structural and functional effects of apolar mutations of the distal valine in myoglobin. *J Mol Biol*. 1995; 245:416–436. [PubMed: 7837273]
45. Wiltrot ME, Giovannelli JL, Simplaceanu V, Lukin JA, Ho NT, Ho C. A biophysical investigation of recombinant hemoglobins with aromatic B10 mutations in the distal heme pockets. *Biochemistry*. 2005; 44:7207–7217. [PubMed: 15882059]
46. Brucker EA. Genetically crosslinked hemoglobin: a structural study. *Acta Crystallogr D Biol Crystallogr*. 2000; 56:812–816. [PubMed: 10930828]
47. Mathews AJ, Rohlfs RJ, Olson JS, Tame J, Renaud JP, Nagai K. The effects of E7 and E11 mutations on the kinetics of ligand binding to R state human hemoglobin. *J Biol Chem*. 1989; 264:16573–16583. [PubMed: 2777799]
48. Esquerra RM, Lopez-Pena I, Tipgunlakant P, Birukou I, Nguyen RL, Soman J, Olson JS, Kliger DS, Goldbeck RA. Kinetic spectroscopy of heme hydration and ligand binding in myoglobin and isolated hemoglobin chains: an optical window into heme pocket water dynamics. *Phys Chem Chem Phys*. 2010; 12:10270–10278. [PubMed: 20668762]
49. Park SY, Yokoyama T, Shibayama N, Shiro Y, Tame JR. 1.25 Å resolution crystal structures of human haemoglobin in the oxy, deoxy and carbonmonoxy forms. *J Mol Biol*. 2006; 360:690–701. [PubMed: 16765986]

50. Schotte F, Soman J, Olson JS, Wulff M, Anfinrud PA. Picosecond time-resolved X-ray crystallography: probing protein function in real time. *J Struct Biol.* 2004; 147:235–246. [PubMed: 15450293]
51. Cassoly R, Gibson Q. Conformation, co-operativity and ligand binding in human hemoglobin. *J Mol Biol.* 1975; 91:301–313. [PubMed: 171411]
52. Olson JS, Phillips GN. Myoglobin discriminates between O₂, NO, and CO by electrostatic interactions with the bound ligand. *J. Biol. Inorg. Chem.* 1997; 2:544–552.

Geminate CO recombination to HbA tetramers

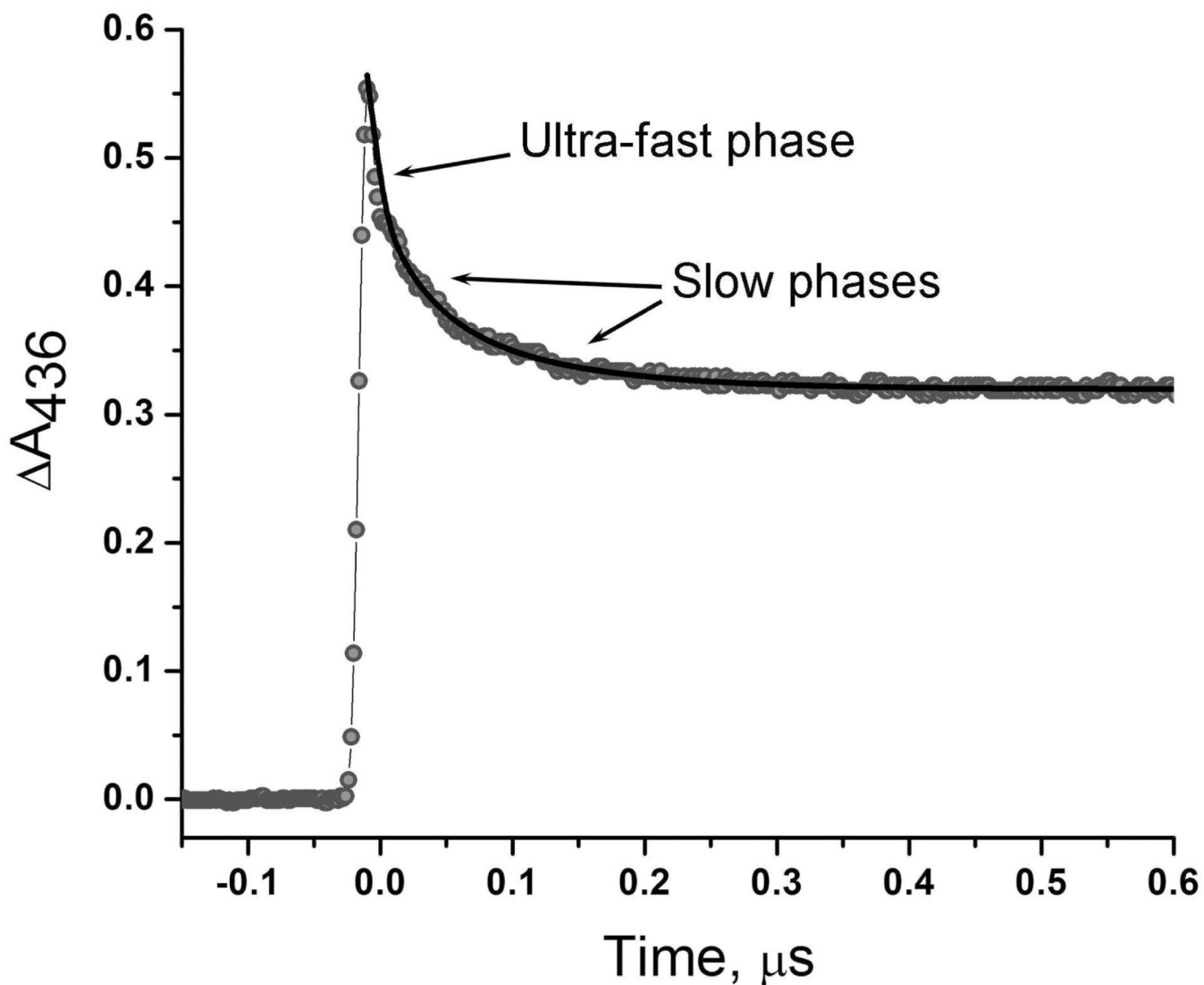
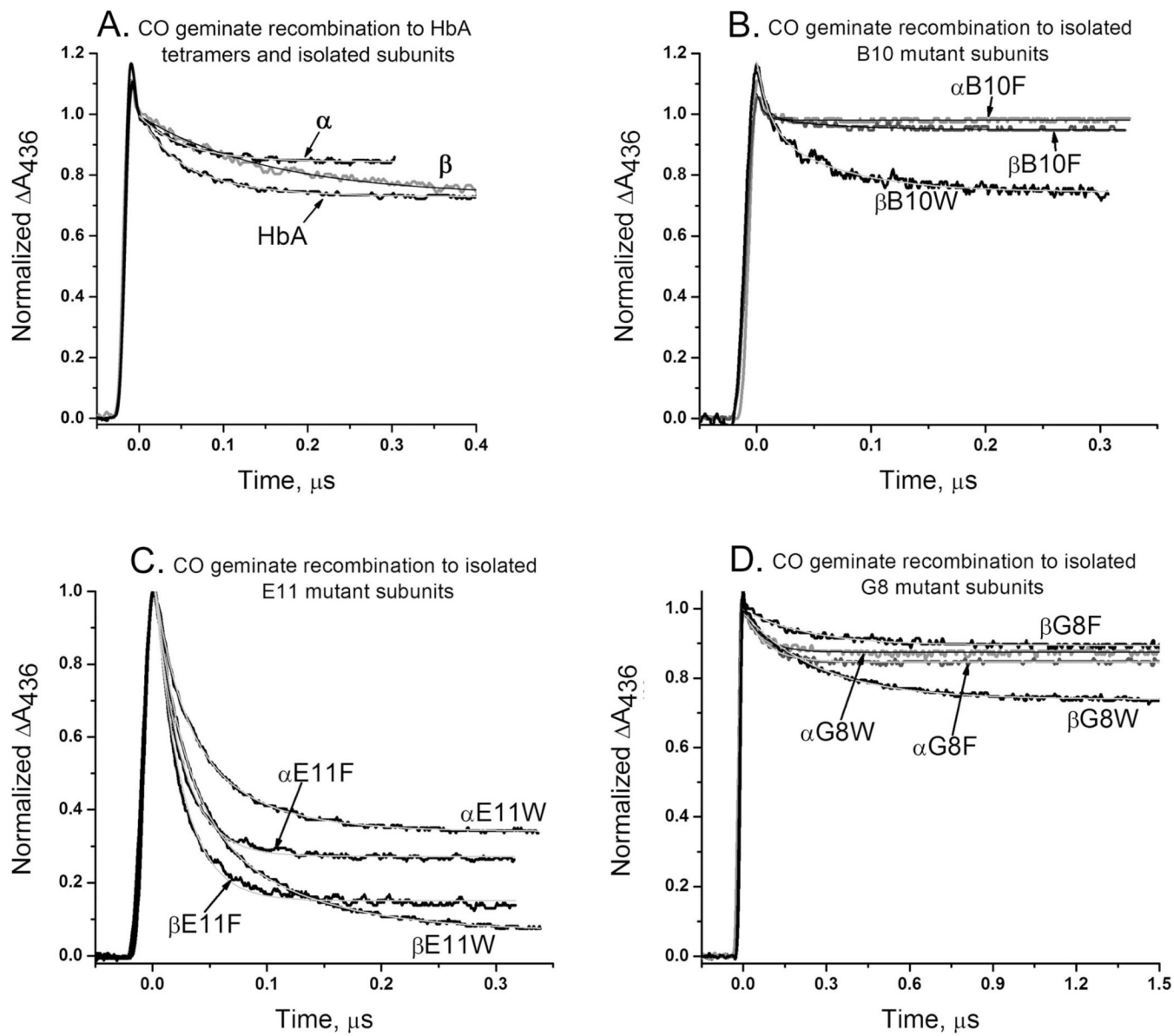


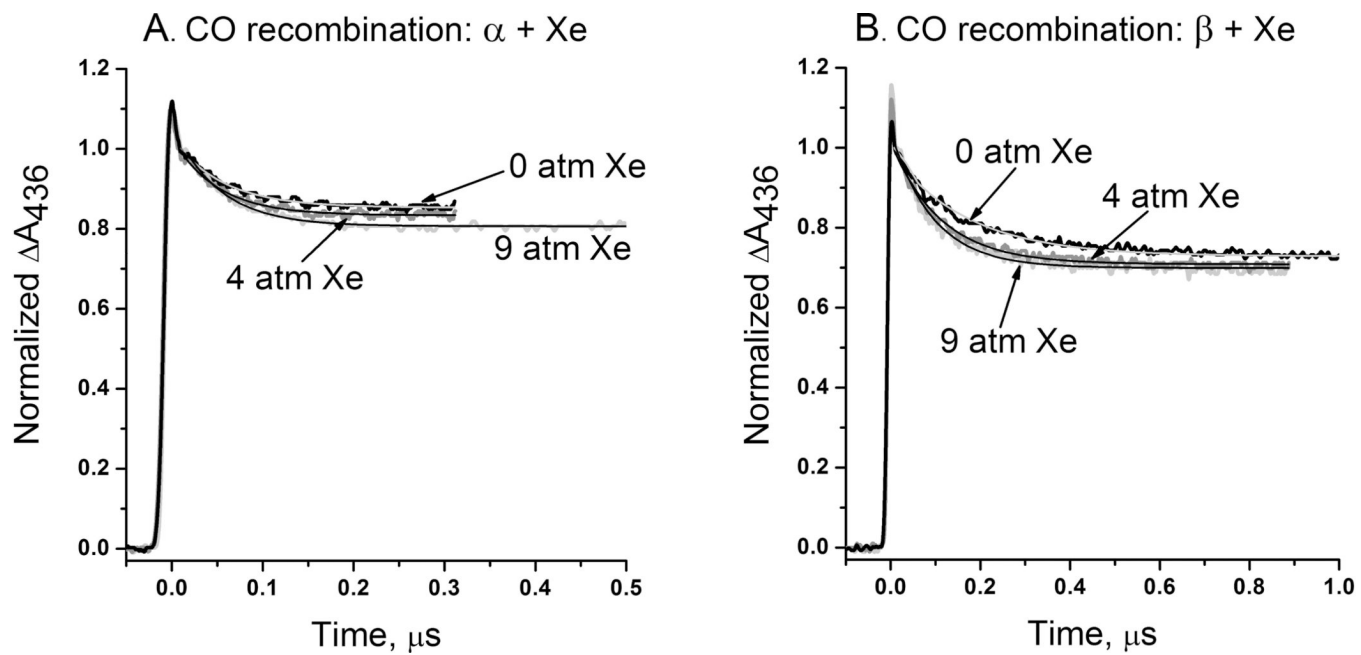
Figure 1.

Ultra-fast and slow phases for CO geminate recombination within tetrameric native HbA. A solution of ~100 μM HbA(CO) in 1000 μM CO, was photolyzed with a 7 ns Nd:YAG laser excitation pulse, and absorbance changes were monitored at 436 nm. The ultra-fast phase represents ligand rebinding from the initial photolyzed complex, which occurs on time scales shorter than ~5–10 ns. The slower geminate phase represents rebinding from within the distal pocket. Measurements were conducted in 100 mM Sodium phosphate, pH 7, 20 °C.

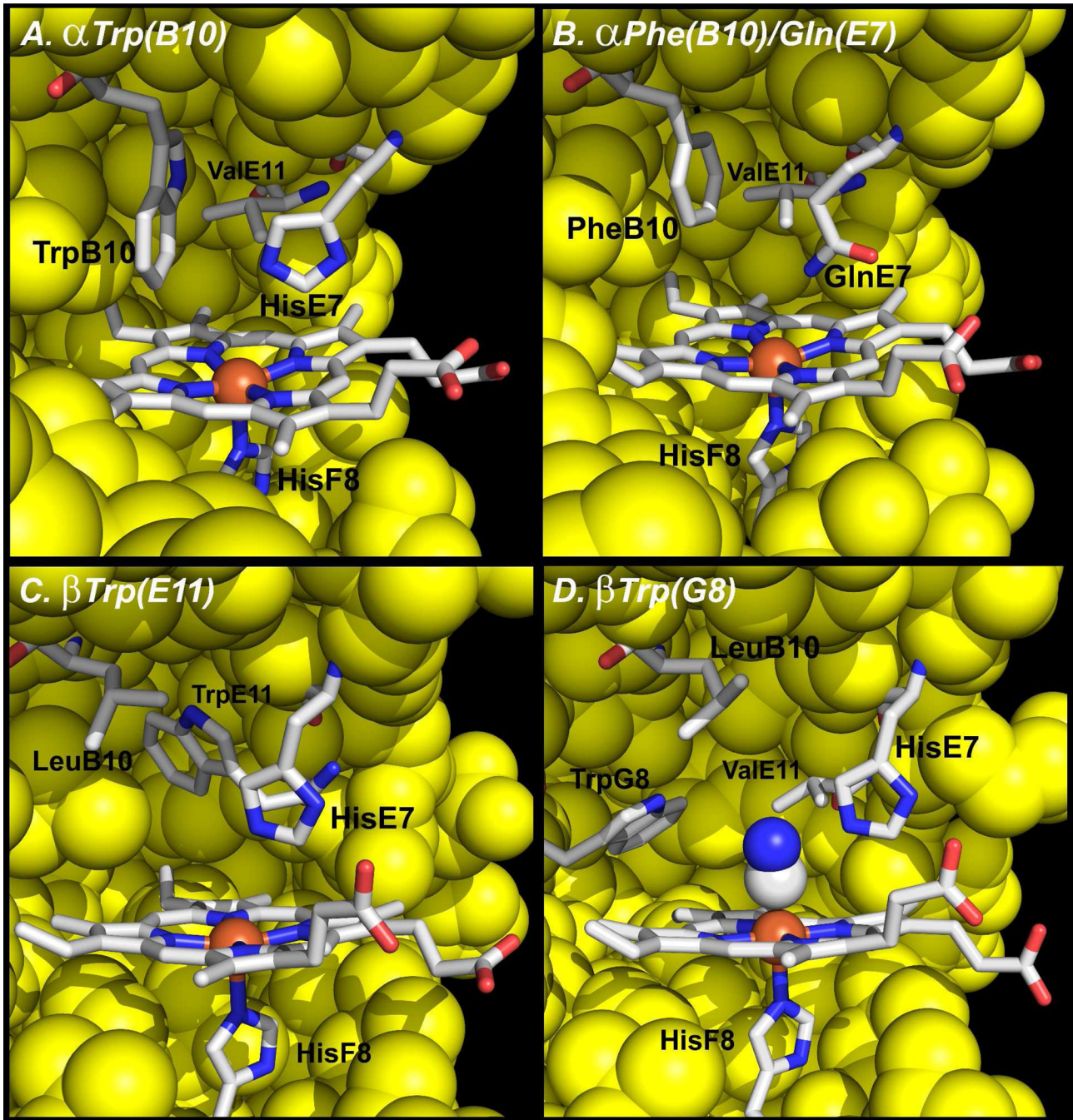
**Figure 2.**

CO geminate rebinding to WT and mutant Hbs. The protein concentrations were kept between 50–100 μM , and $[CO] = 1000 \mu M$. Rates and amplitudes of slow geminate rebinding to subunits within tetramers were obtained by fitting the slow phases to a two-exponential expression, $A(t) = A_{\text{escape}} + A_{\text{gem},a} \exp(-k_{\text{gem},a} t) + A_{\text{gem},b} \exp(-k_{\text{gem},b} t)$; whereas the parameters for slow geminate rebinding in isolated subunits were fitted to a single-exponential expression, $A(t) = A_{\text{escape}} + A_{\text{gem}} \exp(-k_{\text{gem}} t)$. The smooth gray lines represent the best-fitted exponential expression. The time courses were normalized by dividing each observed absorbance change point by the total change measured at 436 nm (excluding the ultra-fast phase). F_{gem} was obtained by dividing A_{gem} by the total ΔA_{436} (or $0.5\Delta A_{436}$ for α or β subunits within a tetramer, because only 50% of the total absorbance change of tetramer corresponds to a particular subunit). k_{gem} is equal to the observed rate of the first order internal rebinding phase. (A) Geminate CO recombination within HbA tetramers and isolated native α and β subunits; (B) geminate CO recombination within isolated B10 mutant

subunits (B10 corresponds to position 29 in α subunits, and 28 in β); (C) geminate CO recombination within isolated E11 mutant subunits (E11 corresponds to position 62 in α subunits, and 67 in β); (D) geminate CO recombination within isolated G8 mutant subunits (G8 corresponds to position 101 in α subunits, and 106 in β). Conditions were the same as in Figure 1.

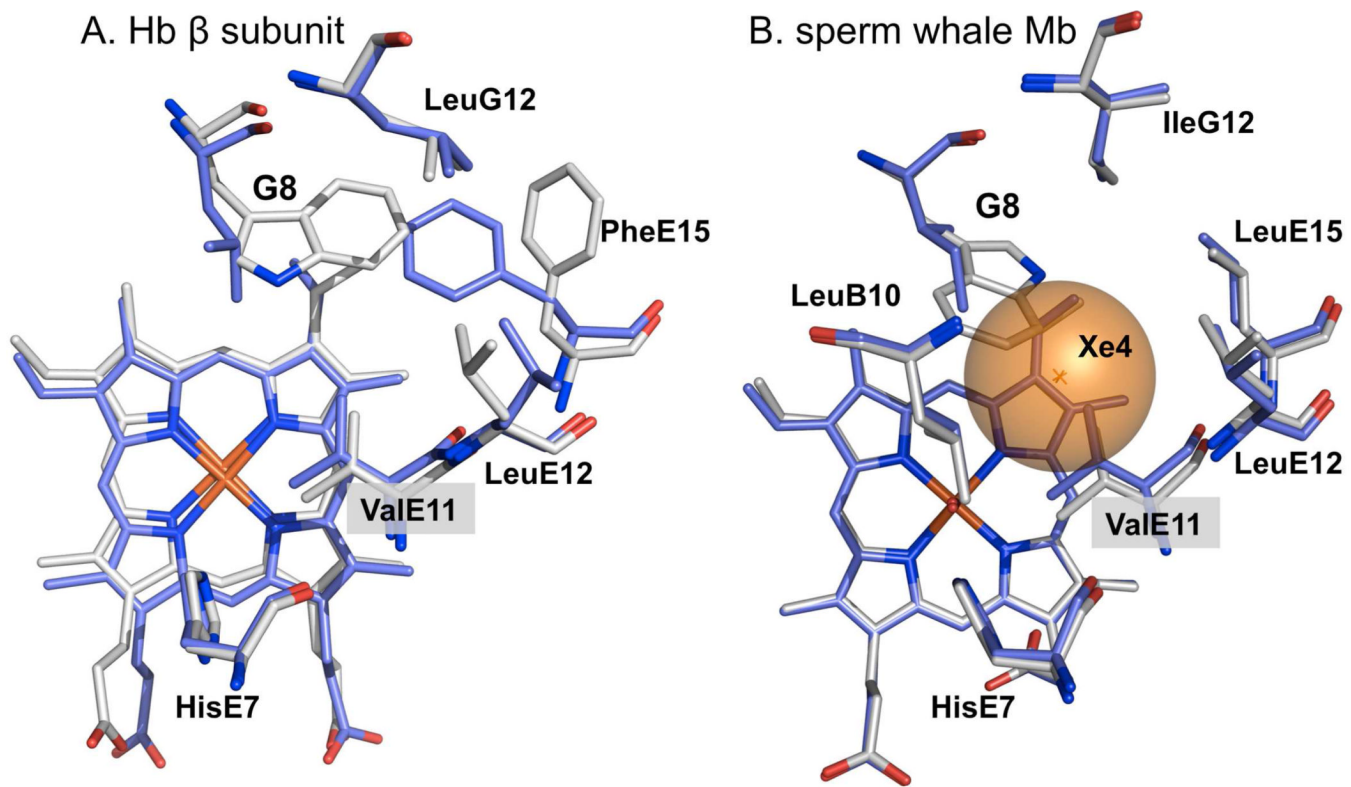
**Figure 3.**

CO geminate rebinding to isolated α (A) and β (B) native subunits in the presence/absence of Xe. Kinetic measurements were conducted in a high-pressure cuvette (see Materials and Methods and (26)) in 1 atm CO plus 0, 4 and 9 atm of Xe. The absorbance changes were normalized for more direct comparisons. The smooth gray lines represent best fits to a single-exponential expression for the slow phase. Experimental conditions were the same as in Figure 1.

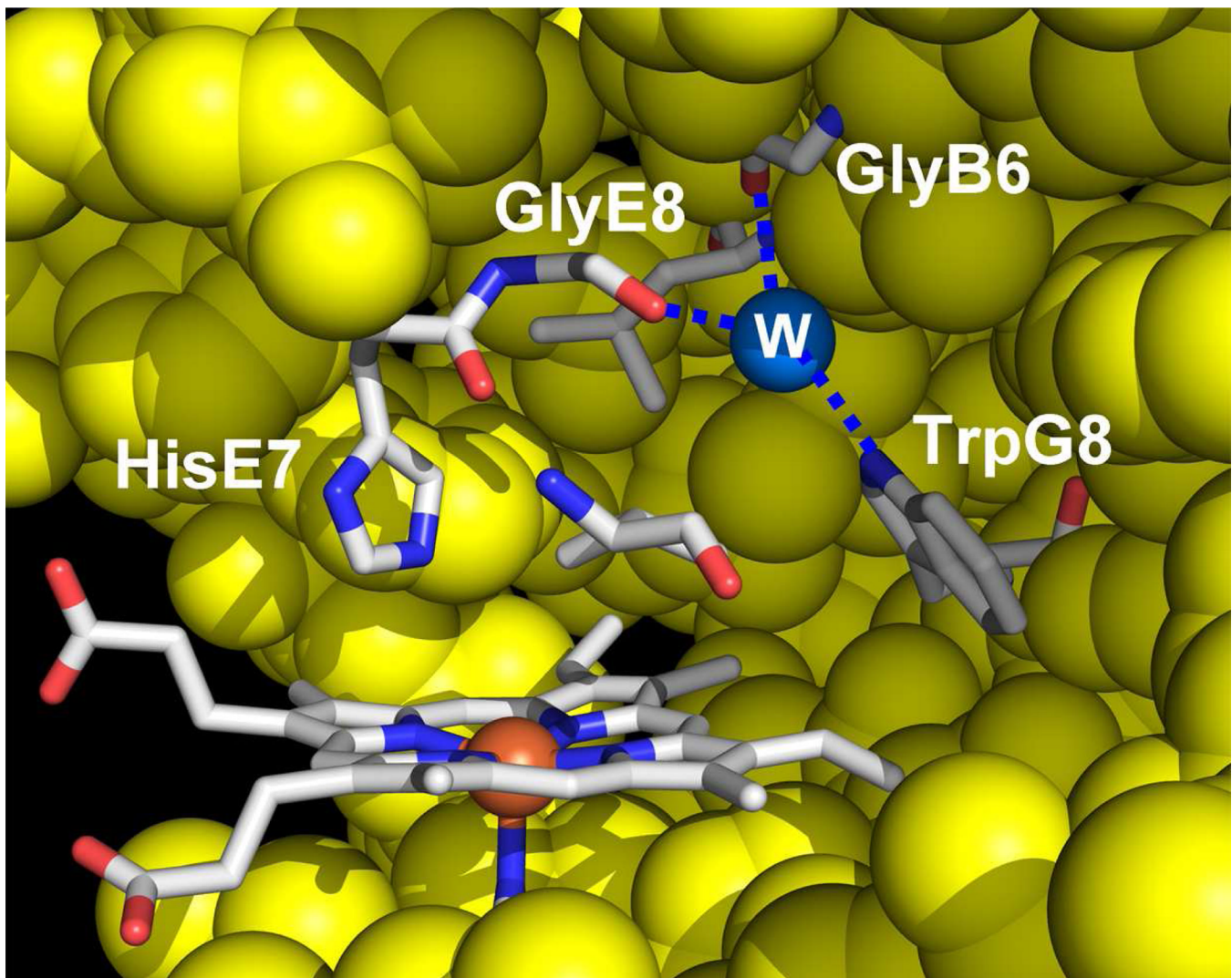
**Figure 4.**

Structures of the key B10, E11 and G8 mutants of HbA. The models of the mutant distal pockets were constructed from the following structures: (A) deoxyHb α (Trp(B10)): β (WT) (1O1N); (B) deoxyHb α (Phe(B10)/Gln(E7)): β (Trp(G8)) (1O1J); (C) deoxyHb α (Phe(B10))/Gln(E7): β (Trp(E11)) (1O1M); and (D) cyanometHb α (Phe(B10)/Gln(E7)): β (Trp(G8)) (1O1I). In addition to the listed mutations, each structure contains Gly links between α chains and Met(NA1) replacements in both subunits. The key residues of the heme pocket are labeled and shown in sticks. The atoms of the key amino acids are colored as following: white, carbon; blue, nitrogen; red, oxygen; yellow, the atoms of other amino acids lining the binding site; and orange, heme Fe. In (D), white and blue spheres represent the CN ligand.

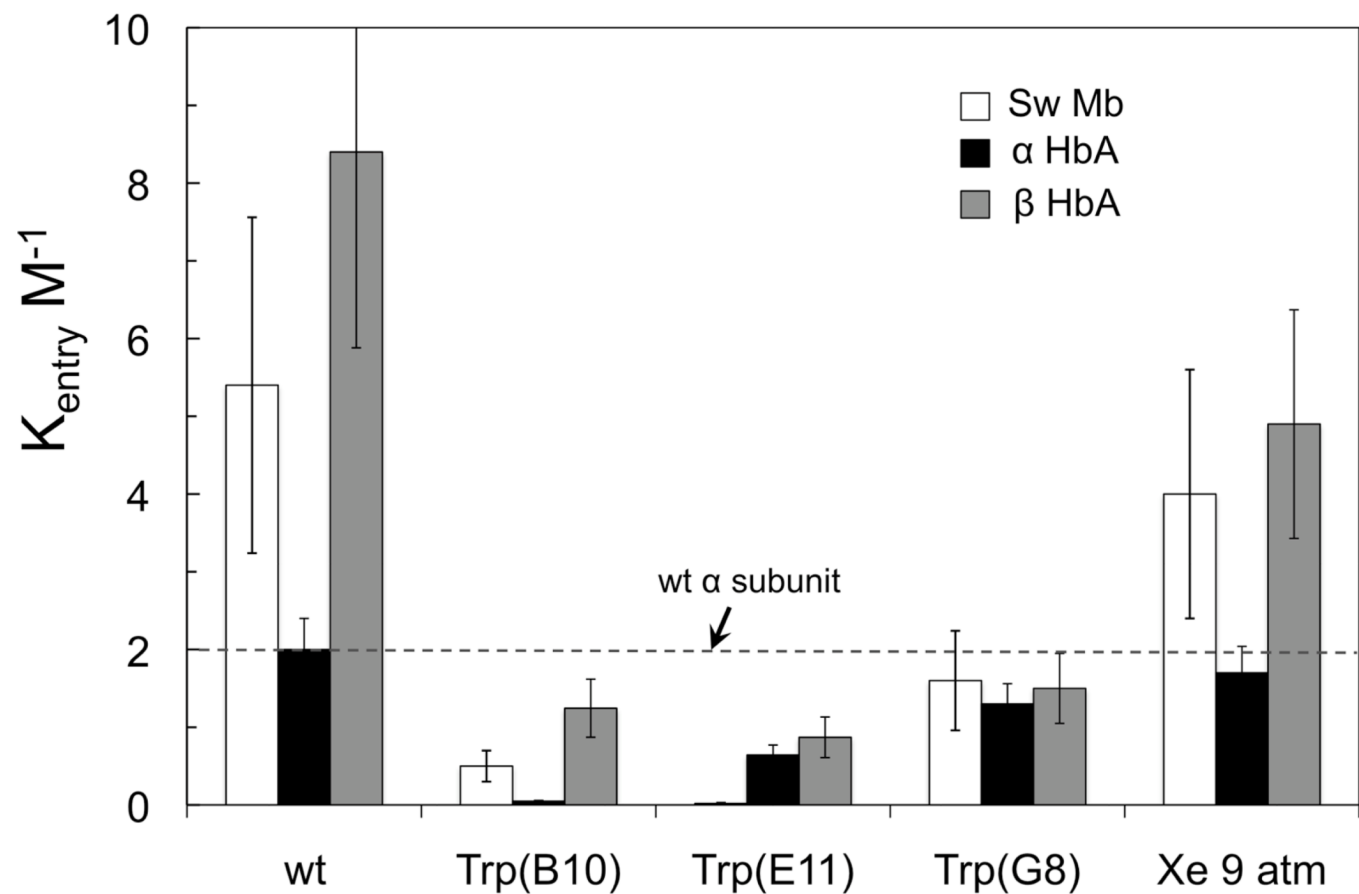
bound to Fe³⁺. In each panel, part of the distal pocket was removed to show the internal structure. All molecular drawings (Figures 4, 5, 6 and 8) were prepared using PyMol (PyMOL Molecular Graphics System, Version 1.2r3pre, Schrödinger, LLC).

**Figure 5.**

Distal pocket structures of **A**, WT β HbO₂ (2DN1) and cyanomet- β (Trp(G8)) (101I) HbA and **B**, WT (2MBW) and Trp(G8) (2OHB) sperm whale aquometMb. The atoms are colored as in Figure 4, except that the carbons are white in the mutant structures and blue in the WT structures for both β subunits and Mb. The large brown sphere in *panel B* represents the Xe4 cavity in sw Mb.

**Figure 6.**

Structure of the deoxy- β Trp(G8) distal pocket. This model was constructed from the structure of deoxyHb α_1 (Met(NA1)/Phe(B10)/Gln(E7))-G- α_2 -(Phe(B10)/Gln(E7)): β (Met(NA1)/Trp(G8)) (1O1J) using PyMol. The blue sphere corresponds to distal pocket water molecule; blue dotted lines represent hydrogen bonds. The atoms are colored as in Figure 4. Part of the distal pocket was removed to show the internal structure.

**Figure 7.**

Effects of Trp mutations and Xe on the equilibrium constant for non-covalent ligand capture (K_{entry}). The errors for the WT values were computed for ≥ 3 independent determinations of K_{entry} , including previous data for both O₂ and CO binding (15, 31, 37). The dashed line represents the value of 2.0 M^{-1} for WT α subunits.

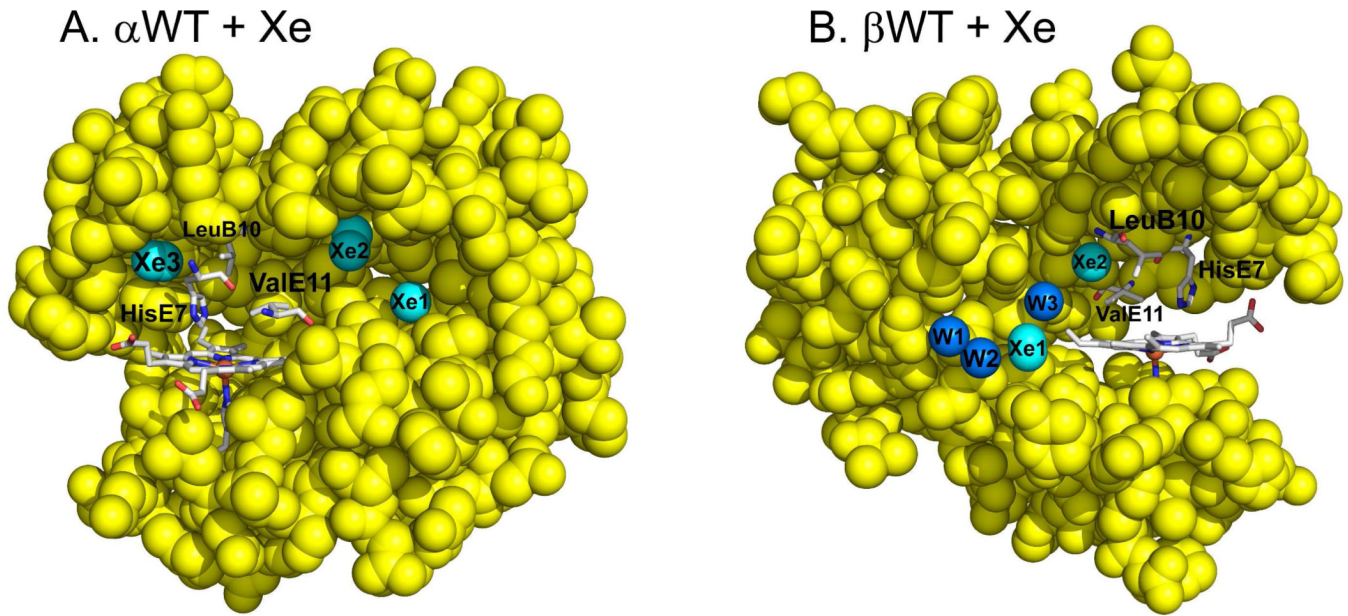
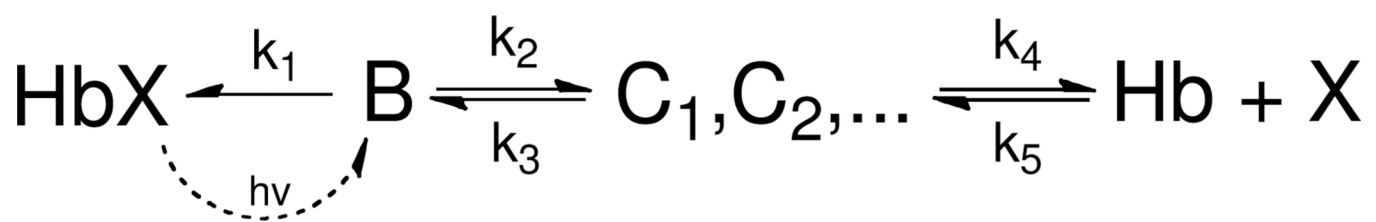
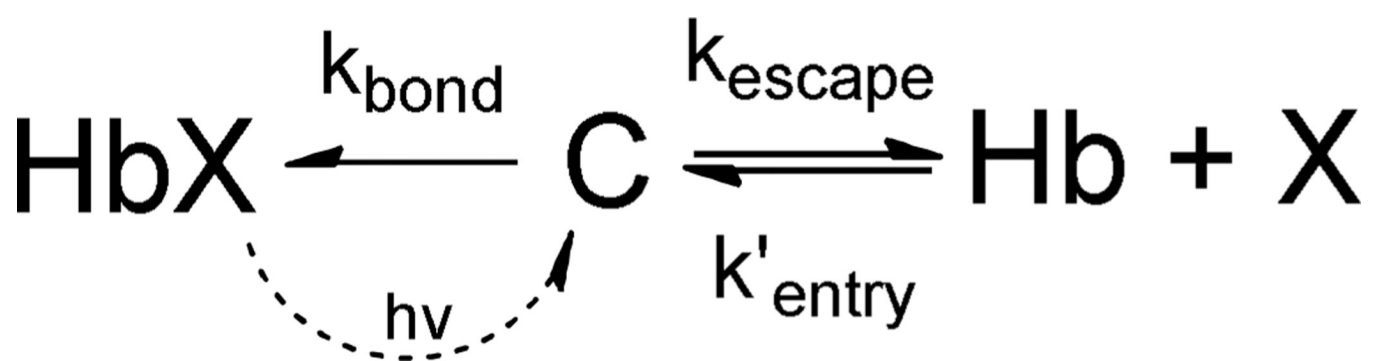


Figure 8.

Structures of the deoxy α (**A**) and β (**B**) subunits with bound Xe atoms. The structures were constructed from the PDB file 2W6V (30). The key residues of the heme pocket are labeled and shown in sticks. The atoms of key amino acids are represented as sticks, colored as in Figure 4. Cyan spheres represent Xe, and the blue spheres indicate positions of water molecules. In the β subunit, water molecules are shown to emphasize possible ligand migration pathways. In *panel B*, W1 and W2 are external waters, whereas W3 and the Xe atoms are buried inside the protein.



Scheme 1.
General four-state geminate rebinding scheme.



Scheme 2.

Two-step geminate rebinding scheme for nanosecond geminate recombination.

Table 1

Geminate parameters of CO recombination to HbA tetramers and isolated subunits.

Subunit	Parameter ¹	Isolated subunit	Tetramer
αWT	$k_{\text{gem}} \mu\text{s}^{-1}$	20 ± 1	34 ± 3
	F_{gem}	0.16 ± 0.01	0.28 ± 0.06
	$k_{\text{bond}} \mu\text{s}^{-1}$	3.1 ± 0.4 $(2.5 \pm 1.0)^2$	9.4 ± 1.3
	$k_{\text{escape}} \mu\text{s}^{-1}$	17 ± 2 $(13 \pm 4)^2$	24 ± 4
βWT	$k_{\text{gem}} \mu\text{s}^{-1}$	7.1 ± 0.6	10 ± 2
	F_{gem}	0.26 ± 0.02	0.33 ± 0.03
	$k_{\text{bond}} \mu\text{s}^{-1}$	1.9 ± 0.3 $(1.7 \pm 0.4)^2$	3.5 ± 0.8
	$k_{\text{escape}} \mu\text{s}^{-1}$	5.3 ± 0.4 $(4.8 \pm 1.0)^2$	7.0 ± 1

¹The geminate parameters were computed using Scheme 2 and Equations 1–3. To compare F_{gem} of isolated subunits to those of subunits within HbA tetramers, F_{gem} for the α and β phases in the tetramer data were divided by 0.5 to normalize for heme concentration (*i.e.* in HbA one half of heme groups are α and the other half are β).

²The values in parentheses were taken from Olson *et al.* (37) and were computed by reducing Scheme 1 to Scheme 2 as described in the text (*i.e.* $k_{\text{bond}} = k_3 k_1 / (k_1 + k_2)$ and $k_{\text{escape}} = k_4$).

Table 2

Rate constants for bimolecular CO, NO, and O₂ binding, NO dioxygenation and parameters for the slow CO geminate recombination to isolated α and β B10 mutant subunits.

Subunit	F _{gem}	k _{gem} μs ⁻¹	k _{bond} μs ⁻¹	k _{escape} μs ⁻¹	k' _{CO} μM ⁻¹ s ⁻¹	k' _{entry} μM ⁻¹ s ⁻¹	K _{entry} M ⁻¹	k' _{NO} μM ⁻¹ s ⁻¹	k' _{NOD} μM ⁻¹ s ⁻¹	k' _{O₂} μM ⁻¹ s ⁻¹
α WT	0.16±0.01	20±1	3.1±0.4	17±2	5.2±0.5 (2.9±1.2)	33±4	2.0±0.2	31	50 ^a (35±10)	40±2
α Phe(B10) ^b	~0	n.d.	n.d.	n.d.	0.032 (0.020)	n.d.	0.27 ^c	4.5	8.0 (3.0)	0.87 (0.64)
α Trp(B10) ^b	~0	n.d.	n.d.	n.d.	0.0033 ^b	n.d.	0.048 ^c	0.81 ^d	1.6 ^d (0.10)	0.033 (0.10)
β WT	0.26±0.02	7.1±0.6	1.9±0.3	5.3±0.4	11±3.3 (6.8±1.5)	42±13	8.4±2.0	68	50 ^a (67±9)	63±12
β Phe(B10)	0.04	19	0.81	18	1.6 (48%) 0.27 (52%) (0.32)	37 6.3 0.35	2.1 0.35	57	~100 ^e (50)	26 (56%) 5.8 (44%) (8.2)
β Trp(B10)	0.22	15	3.4	12	5.1 (62%) 0.0029 (38%) (0.0016)	23 0.013	2.0 0.011	22 (56%) 0.34 (44%)	50 (72%) 3.7 (28%) (0.033)	23 (58%) 0.013 (42%)

The naturally occurring amino acid at the B10 position is Leu in both subunits. In cases where two bimolecular binding phases were observed for isolated subunits, the relative percentages of each phase are indicated in parentheses. Parameter values were rounded to two significant digits. K_{entry} and K_{entry} were calculated or estimated using the expressions in Equation 1. k_{gem}, k_{bond} and k_{escape} for α Phe(B10) and α Trp(B10) were not determined, because F_{gem} ≈ 0. K'CO and K'O₂ for WT α and β chains were taken from Birukou *et al.* (2010) (31). The values in parentheses for k'CO and k'O₂ are for subunits within tetramers taken from (43). k'NOD values in parentheses for α and β Phe(B10) variants in tetramers taken from (34). Conditions were the same as in Figure 1.

^ak'NOD for α and β WT subunits within HbA tetramers.

^bGeminate and bimolecular binding parameters are for α Trp(B10) subunits within hybrid mutant/WT tetramers.

^ck'NO was used as the rate of ligand entry for α Trp(B10), and the wild-type α parameter was used for the rate of ligand escape.

^dThe amplitude of the slow phase in both NO dioxygenation and bimolecular NO binding was less than 0.5 of the total absorbance change. The fast phase parameters for the hybrid HbA tetramers agreed well with and were assigned to the wild-type β subunits.

^eThe rate of reaction was too fast to be reliably measured.

Rate constants for bimolecular CO, O₂, and NO binding, NO dioxygenation, and CO geminate recombination for isolated α and β E11 mutant subunits.**Table 3**

Subunit	F _{gem}	k _{gem} μs ⁻¹	k _{bond} μs ⁻¹	k _{escape} μs ⁻¹	k' _{CO} μM ⁻¹ s ⁻¹	k' _{entry} μM ⁻¹ s ⁻¹	K _{entry} M ⁻¹	k' _{NO} μM ⁻¹ s ⁻¹	k' _{NOD} μM ⁻¹ s ⁻¹	k' _{O₂} μM ⁻¹ s ⁻¹
α WT	0.16±0.01	20±1	3.1±0.4	17±2	5.2±0.5 (2.9±1.2)	33±4	2.0±0.2	31	50 ^a	40±2 (35±10)
α Phe(E11)	0.73	43	31	12	4.0 (3.7)	5.5	0.47	18	42	10 (19)
α Trp(E11)	0.37 (56%) 0.29 (44%) <i>total</i> =0.67	17 48	6.2 14	11 34	4.6 (50%) 0.85 (50%) (2.1)	1.3 2.9	1.2 0.086	23 (67%) 3.1 (33%)	43	11 (6.1%) 1.3 (39%) (16)
β WT	0.26±0.02	7.1±0.6	1.9±0.3	5.3±0.4	11±3.3 (6.8±1.5)	42±13	8.4±2.0	68	50 ^a	63±12 (67±9)
β Phe(E11)	0.85	43	37	6.5	7.8 (7.0)	9.2	1.4	21	23	19 (12)
β Trp(E11)	0.30 (44%) 0.65 (56%) <i>total</i> =0.95	8.2 36	2.4 23	5.8 13	4.5 (30%) 1.0 (70%) (5.9)	15 1.6	2.6 0.13	8.3 (46%) 2.3 (54%)	9.4 2.1 (62%)	8.8 (38%) (14)

WT α and β subunits have valine at the E11 position. In cases where multiple bimolecular binding phases were observed, parameters for both processes are presented and relative contributions of each phase are shown in parentheses. Parameter values were rounded to two significant digits, in the case of equilibrium constants after ratios were calculated. K_{entry} was calculated using the formula K_{entry}=k'_{entry}/k'_{escape}. k'_{CO} and k'_{O₂} columns, the values in parentheses represent the parameters for subunits within tetramers taken from (43). The k'_{NOD} values in parentheses are for α Phe(E11) and β Phe(E11) mutants within tetramers taken from (34). Conditions were the same as in Figure 1.

^a k'_{NOD} for WT α and β subunits within HbA tetramers.

Table 4

Rate constants for bimolecular CO, O₂, and NO binding, NO dioxygenation, and CO geminate recombination to isolated α and β G8 mutant subunits.

Subunit	F _{gem}	k _{gem} μs ⁻¹	k _{bond} μs ⁻¹	k _{escape} μs ⁻¹	k' _{CO} μM ⁻¹ s ⁻¹	k' _{O₂} μM ⁻¹ s ⁻¹	K _{entry} M ⁻¹	k' _{NO} μM ⁻¹ s ⁻¹	k' _{O₂} μM ⁻¹ s ⁻¹
α WT	0.16±0.01	20±1	3.1±0.4	17±2	5.2±0.5 (2.9±1.2)	33±4	2.0±0.2	31	50 ^a (35±10)
α Phe(G8)	0.15	13	2.0	11	3.6 (2.3)	24	2.1	40	55 (22)
α Trp(G8)	0.12	14	1.7	12	2.0 (1.5)	16	1.3	30	74 (13)
β WT	0.26±0.02	7.1±0.6	1.9±0.3	5.3±0.4	11±3.3 (6.8±1.5)	42±13	8.4±2.0	68	50 ^a (67±9)
β Phe(G8)	0.12	5.2	0.60	4.6	2.2 (1.0)	19	4.2	41	75 (19)
β Trp(G8)	0.26	3.8	0.97	2.8	1.1 (0.42)	4.3	1.5	10	15 (4.2)

WT α and β subunits both have leucine at the G8 position. All values, calculated or measured, were rounded to 2 significant digits. Kentry was calculated as Kentry=k'entry/k_{escape}. k'_{CO} and k'_{O₂} for WT α and β chains were taken from Birukou *et al.* (31). The values in parentheses in the k'_{CO} and k'_{O₂} columns represent the parameters for subunits within tetramers taken from (43). Conditions were the same as in Figure 1.

^a k'NOD values for α and β WT subunits within HbA tetramers.

Table 5

The effect of Xe on kinetic parameters for bimolecular CO and O₂ binding and CO geminate recombination to isolated α and β subunits.

Subunit	F _{gem}	k _{gem} μs ⁻¹	k _{bond} μs ⁻¹	k _{escape} μs ⁻¹	k' _{CO} μM ⁻¹ s ⁻¹	k' _{entry} μM ⁻¹ s ⁻¹	K _{entry} M ⁻¹	k' _{O₂} μM ⁻¹ s ⁻¹
$\alpha + 0$ atm Xe	0.16 ± 0.01	20 ± 1	3.1 ± 0.4	17 ± 2	5.8 ± 0.2	37 ± 3	2.2 ± 0.3	45 ± 3
$\alpha + 4$ atm Xe	0.19 ± 0.01	19 ± 1	3.7 ± 0.5	16 ± 2	6.1 ± 0.2	31 ± 2	2.0 ± 0.3	42 ± 3
$\alpha + 9$ atm Xe	0.24 ± 0.01	20 ± 1	4.8 ± 0.5	15 ± 1	6.0 ± 0.1	25 ± 2	1.7 ± 0.1	41
$\beta + 0$ atm Xe	0.26 ± 0.02	7.1 ± 0.6	1.9 ± 0.3	5.3 ± 0.4	15 ± 0.2	56 ± 5	1.1 ± 1	74 ± 2
$\beta + 4$ atm Xe	0.29 ± 0.02	8.8 ± 1.2	2.5 ± 0.6	6.3 ± 1.8	13 ± 0.2	45 ± 4	7.1 ± 2.1	65 ± 1
$\beta + 9$ atm Xe	0.30 ± 0.02	11 ± 1	3.2 ± 0.6	7.4 ± 2.1	11 ± 0.3	36 ± 3	4.9 ± 1.4	59

Average parameter values ± standard deviations are presented when three separate experiments (on different days with different protein samples) were performed. Parameter values were rounded to two significant digits after all calculations. K_{entry}=k_{entry}/k_{escape}. Experimental conditions were the same as in Figure 1. In this table, only the results for O₂ and CO bimolecular binding conducted in the high pressure stainless steel cuvette were used to calculate the mean values and standard deviations for k'_{entry}, k'_{O₂} and k'_{CO}. The fitted parameters for 0 atm Xe are not statistically different from those for α WT and β WT subunits reported in Tables 1–4 and (31).

Table 6

The effect of Xe on the kinetic parameters for geminate CO recombination to R state HbA tetramers and on the bimolecular association rate constant for CO binding T state deoxyHbA.

Subunit	F_{gem}	$F(\alpha + \beta)$	k_{gem} μs^{-1}	k_{bond} μs^{-1}	k_{escape} μs^{-1}	k'_{TCO} $(\alpha + \beta)$ $\mu\text{M}^{-1}\text{s}^{-1}$
Hb $\alpha + 0$ atm Xe	0.28 ± 0.06	0.31 ± 0.03	34 ± 3	9.4 ± 1.3	24 ± 4	
Hb $\beta + 0$ atm Xe	0.33 ± 0.03		10 ± 2	3.5 ± 0.8	7 ± 1	0.24 ± 0.01
Hb $\alpha + 4$ atm Xe	0.43 ± 0.07	0.37 ± 0.04	30 ± 3	13 ± 2	17 ± 2	
Hb $\beta + 4$ atm Xe	0.32 ± 0.06		9.9 ± 3	3.2 ± 1.1	6.7 ± 1.7	0.22
Hb $\alpha + 9$ atm Xe	0.44 ± 0.05	0.42 ± 0.02	33 ± 3	15 ± 1	18 ± 3	
Hb $\beta + 9$ atm Xe	0.38 ± 0.04		11 ± 1	4 ± 1	6.5 ± 0.8	0.24

When three or more independent experiments were conducted, the measured or calculated parameters are presented as the mean value ± standard deviation. Parameter values were rounded to two significant digits. $F(\alpha + \beta)$ represents the average of F_{gem} for α and β subunits within the tetramer, represents the total fraction of geminate recombination observed for the Hb sample. The F_{gem} values for the individual subunits were calculated as $A_{\text{gem}}(\alpha \text{ or } \beta)/0.5$, where $A_{\text{gem}}(\alpha \text{ or } \beta)$ is the observed amplitude of geminate rebinding assigned to an individual α or β subunit within a tetramer. The experimental conditions were the same as in Figure 1.